**Doctoral Thesis**

# Dual Anti-tumorigenic Activities of Human Glycyl-tRNA Synthetase and Its Peptide Derivatives

# Glycyl-tRNA Synthetase 와 펩타이드의 항암효과에 관한 연구

**February 2018**

**Graduate School of Convergence Science and Technology**

**Department of Molecular Medicine and Biopharmaceutical Sciences**

**Peter Goughnour**

# Dual Anti-tumorigenic Activities of Human Glycyl-tRNA Synthetase and Its Peptide Derivatives

# Glycyl-tRNA Synthetase 와 펩타이드의 항암효과에 관한 연구

**Professor Sunghoon Kim**

**Submitting a Doctoral Thesis of Pharmacology**

**February 2018**

**Graduate School of Convergence Science and Technology**

**Department of Molecular Medicine and Biopharmaceutical Sciences**

**Peter Goughnour**

**Confirming the doctoral thesis written by Peter Goughnour**

**February 2018**

**Chair_____ (Seal)**

**Vice Chair_____ (Seal)**

**Examiner_____ (Seal)**

**Examiner_____ (Seal)**

**Examiner_____ (Seal)**

# ABSTRACT

Over the past decade, the ex-translation functions of secreted Aminoacyl-tRNA Synthetases (AARSs) have been more elucidated. Several of the secreted AARSs have been shown to be correlated to the immune system. Secreted Tryosyl-tRNA Synthetase (YRS) and Histidyl-tRNA Synthetase (HRS)/Asparaginyl-tRNA Synthetase (NRS) induce polymorphonuclear leukocyte (PMN) and immature dendritic cell migration, respectively.

In relation to macrophage, Tryptophanyl-tRNA Synthetase (WRS) plays a role in activating macrophage upon bacterial infection while Lysyl-tRNA Synthetase (KRS) and Glycyl-tRNA Synthetase (GRS) were both shown to have an influence on macrophages in a tumor microenvironment. KRS secretion from tumor cells causes a proinflammatory response and migration of macrophage. GRS secretion from macrophage responds to Fas ligand secreted from tumor cells and binds to Cadherin-6 (CDH6) suppressing tumor growth.

Previous observations showed that GRS antibodies were detected in patients' blood with inflammatory induced myositis and interstitial lung disease. In addition, GRS was shown to bind to macrophage, which mediates inflammatory

responses. These observations lead me to further understand the role of GRS on macrophage. In this study, I focused on explicating GRS role on macrophage and development of its derived peptides .

In chapter one of this study, it was shown that macrophage, under stressed conditions, secret GRS in autocrine manner stimulating their polarization to become anti-tumor. GRS binds to macrophage receptor CELSR2, part of the super cadherin and G protein-coupled receptor (GPCR) families, activating the RAS-RAF-MEK signaling pathway. Upon activation, TNF-α, IL-6, and CXCL10 cytokines are secreted shifting macrophages from M0 state to M1 type, which is antitumor, and induces phagocytosis. GRS treatment in an initiation mice model, the growth of tumor was prevented or retarded. This data shows that GRS is an important secreted cytokine that is needed for immune surveillance.

In chapter two of this study, the active domain of GRS that binds to cancer cells was discovered and developed into a druggable peptide. GRS has been previously reported to kill cancers that expressed cadherin-6 (CDH6) by suppressing ERK signaling and inducing apoptosis. Through computational predicted binding regions of GRS to CDH6, mutations were performed to find the

active region of GRS. Upon these results, synthesized peptides were derived and tested *in-vitro* and *in-vivo*. The active region of the peptide was reduced to a conformational stable 8 and cyclic 25 amino acid, which greatly reduced the tumor growth by intra-tumor (IT) and intravenous (IV) injection. *In-vivo* imaging system (IVIS) showed the fluorescent labeled peptides targeting the tumor. These results show a developed GRS-derived peptide role as a potential drug candidate.

This study shows secreted GRS has an important role in immunosurveillance. GRS is secreted by macrophages as an alarmin that notices the abnormal environment formed during tumorigenesis. Secreted GRS polarizes macrophage to produce antitumor cytokines to eliminate the malignant tumor cells and protect the body. In addition, an active and stable peptide derived from GRS was developed. The *in-vitro* and *in-vivo* testing showed promising results that GRS-derived peptide as a therapeutic agent against cancer.

Keywords : Glycyl-tRNA Synthetase, Macrophage, Cancer, Peptide, Therapeutic drug, Cadherin-6, CELSR2

Student ID : 2010-31389

# CONTENTS

**Chapter 2. Development of Glycyl-tRNA Synthetase Derived Peptides with Anti-cancer Activity**

# LIST OF FIGURES

**Chapter 1. Anti-tumor Polarization of Macrophage by Glycyl-tRNA Synthetase**

**Chapter 2. Development of Glycyl-tRNA Synthetase Derived Peptides with Anti-cancer Activity**

# ABBREVIATION LIST

GRS: Glycyl-tRNA Synthetase

KRS: Lysyl-tRNA Synthetase

CELSR2: Cadherin EGF LAG Seven-Pass G-Type Receptor 2

ELISA: Enzyme-linked immunosorbent assay

IL6: Interleukin-6

CXCL10: C-X-C motif chemokine 10

TNF-α: Tumor necrosis factor alpha

FACS: Fluorescence-activated cell sorting

MHCII: Major histocompatibility complex II

CD206: Cluster of Differentiation 206

F4: GRS fragment 4

CDH6: Cadherin-6

PP2A: Phosphatase 2A

HADDOCK: High ambiguity Driven protein-protein DOCKing

CCK8: Cell Counting Kit-8

# CHAPTER 1

# Anti-tumor Polarization of Macrophage by Glycyl-tRNA Synthetase

**Keywords** : Glycyl-tRNA Synthetase, Macrophage, Cancer, CELSR2

# INTRODUCTION

Tumor-associated macrophages (TAM) are classified to classically activated (M1) and alternatively activated (M2) subtypes depending on their roles in tumor growth and processes. In tumor microenvironment, M1 type macrophages are tamed by cancer-released factors to become M2 type that stimulates tumor angiogenesis, growth, metastasis, and immunosuppression(Gordon and Martinez, 2010). However, it is not well known how the fate of macrophages is determined in tumor microenvironment.

Cadherin EGF LAG seven-pass G-type receptors (CELSR) is a unique type of receptor. It belongs to both cadherin superfamily and the G protein-coupled receptor (GPCR) family. CELSRs are important for neuronal system development and male fertility (refxx). Mutations in CELSRs have been associated with human diseases such as breast cancer.(refxx) The CELSR have large ectodomains that consist of cadherin repeats. Since CDH6 has been shown to bind to GRS, CELSR2 may also have the possibility to be a receptor for GRS.

DuringAminoacyl- tRNA Synthetase (AARSs) are enzymes that ligate the appropriate amino acids onto their respective tRNA. Secreted human Tyrosyl-tRNA Synthetase (YRS) is a 528 amino acid protein, which is cleaved into N-

terminal of 364 amino acids and C-terminal of 164 amino acids. This shortened N-terminal peptide, called mini-YRS, functions as an angiogenetic factor while C-terminal peptide, which includes endothelial-monocyte-activating polypeptide II (EMAPII), functions as an immune stimulant. Also Tryptophanyl-tRNA Synthetase (WRS) has two different functions. Full length WRS is secreted from monocytes activating macrophage and the truncated N-terminal peptide has angiostatic cytokine activity.

These finding encouraged us to investigate whether the secreted GRS would have additional roles in macrophage, particularly in the control of M1 and M2 polarization. The functional significance of GRS for macrophage activation and tumor suppression was demonstrated *in vitro* and *in vivo*. This work thus not only characterized the functional receptor, but also its implication for M1 polarization of macrophages in immunological suppression of tumor initiation. 7

# RESULTS

**Secreted GRS induces M1 macrophage markers and activity**

To understand the effect of GRS on macrophage activities, RAW264.7 were treated with GRS and determined the profile of the induced cytokines using multiplex cytokine array. The cytokines known to induce M1 polarization (Mantovani et al., 2004b; Mosmann and Coffman, 1989), such as CXCL10, IL-6 and TNF- α(Gajewski et al., 2013) , were significantly increased (Figure 1A). The transcriptional level of TNF-α in RAW264.7 cells treated with GRS or LPS was higher compared to IL-10 (Figure 1B). ). Primary macrophages were used to validate the effect of GRS on the secreted and transcription level of TNF-α, which dramatically increased with the addition of GRS or LPS relative to IL-10 (Figures 1C and D). The effect of GRS on the expression level of macrophage polarization markers such as MHCII, presenting antigen to adaptive immune cells (M1 marker)(Ziegler-Heitbrock et al., 1993), and CD206 (M2 marker)(Movahedi et al., 2010), by western blot and FACS analyses. In both assays, it was observed that GRS increased surface levels of MHCII similar to LPS (Figures 1E and F). In addition, GRS induced nitric oxide synthase (iNOS) but had no effect on arginase-

1 (Arg I) that are also the known M1 and M2 markers, respectively(Sica and Mantovani, 2012) (Figure 1G).

**Secreted GRS induces TNF-α secretion**

To determine whether GRS would be a major factor for the induction of M1 cytokines in cancer microenvironment, GRS was pre-incubated with anti-GRS antibody, GRS-induced TNF-α secretion was significantly reduced (Figure 2A). Using a transwell (pore size: 0.4 μm), RAW264.7 were seeded in the upper chamber and H460 cells in the lower chamber in the presence or absence of anti-GRS antibody and found that TNF-α secretion was significantly reduced by anti-GRS antibody (Figure 2B). Next, GRS was tested to see induced TNF-α *in-vivo*, so cadherin positive (SN12C upper-right and H460 middle-bottom)and negative cell lines (RENCA) were transplanted. GRS was shown to be secreted in the blood before TNF-α. All of these results suggest that GRS would enhance the production of the M1-type signature cytokines from macrophages and play a crucial role in M1 polarization of cancer-associated macrophages.

**GRS induced phagocytosis in macrophage**

Since phagocytic activity is also one of the hallmarks for M1 macrophages, GRS was tested to see if it would stimulate phagocytic activity of macrophages by incubating macrophages with green fluorescence phagocytosis beads, and observed

the increased phagocytic activity of GRS or LPS treated RAW264.7 cells by microscopy and quantified. (Figure 3A and B) Phagocytosis increased in dose-dependent manner and was confirmed with primary cells (Figure 3C). Next the effect of GRS on phagocytosis-stimulating activity *in vivo* was examined using intravital monitoring system as previously described(Choe et al., 2013). For this experiment, LysM-GFP mouse was used in which macrophages/neutrophils can be monitored by GFP(Faust et al., 2000). This intravital phagocytosis system was validated by injecting LPS as immune stimulant. Significant increase of phagocytic activity was increased by macrophages/neutrophil as shown by LPS treatment (Figure D, left figure), further confirming the role of GRS in M1 polarization of macrophages. The Z stack analysis further confirmed the exact co-localization of macrophages/neutrophil (green) with beads (red) upon treatment with GRS and GRS-EV (Figure D, right figure)

**The M1 polarization of GRS is dependent on RAS-RAF-MEK signaling**

It has been shown that cadherins regulate MAPK signaling (Park et al., 2012; Pece and Gutkind, 2000) and that MAPK signals are known to be critical for TNF-α secretion in macrophages(Means et al., 2000), which is a critical factor for macrophage M1 polarization(Saccani et al., 2006). To identify the GRS signal mediators, the effect of GRS on the activation of RAS-RAF-MEK pathway was

determined by immunoblotting. (Figure 4A). The JAK-STAT pathway is critical for determining if macrophage polarizes to M1 or M2 marker. p-STAT-1 is expressed for M1 macrophage and p-STAT3 is expressed for M2 macrophage (Figure 4B). To see if the GRS activation of M1 macrophages followed a different pathway than LPS.. LPS has been show to activate TNF-α secretion throught NF-kB pathway. Immunoblotting was performed and it is shown that LPS activates the NF-kB while GRS showed no effect (Figure 4C). When macrophage was treated with MEK pathway, p-STAT-1 showed no activation and LPS treatment slightly reduced the p-STAT1. (Figure 4D). Next, macrophage was treated with MEK inhibitor then GRS or LPS to see if the TNF-α secretion was reduced and lose its ability to perform phagocytosis. MEK inhibition reduced TNF-α secretion and phagocytosis with GRS treatment but little effect was shown. (Figure 4E,F) This data confirms that macrophage polarization is dependent on the MEK pathway. In addition, LPS has little effect with MEK inhibition showing the GRS and LPS activate macrophage by different means.

**CELSR2 is identified as receptor for secreted GRS in macrophage**

To see the macrophage binding of GRS, RAW264.7 cells were treated with Alexa-fluor 647 (red fluorescence)-labeled GRS and BSA and observed that only GRS, but not BSA, bound to the cell surface (Figure 5A). Previously identified K-

cadherin (CDH6) was reported as the functional receptor for the death-inducing activity of GRS to cancer cells. Since GRS showed a different activity in macrophages, it was suspected that the functional receptor for GRS in macrophages differed. Potential GRS-binding proteins were searched from PharmDB database that shows the interactions of human proteins (Lee et al., 2012). The database suggested 32 proteins, which only CELSR2 (cadherin EGF LAG seven-pass G type receptor 2) was a membrane protein. CELSR2, part of the cadherin superfamily, was first identified in drosophila (Usui et al., 1999), and its role in planar cell polarity (PCP), which is important for cell shape, structure, migration and function. However, its function in macrophages was not unveiled yet. CELSR2 was expressed in RAW264.7 cells but not in H460 cells. Interestingly, GRS showed preferential binding to CELSR2 in RAW264.7 cells although CELSR2 was detected in both of RAW264.7 and H460 cells (Figure 5B). This result suggests the possible involvement of additional factor(s) that would endow the specific binding of GRS to CELSR2 in macrophages.

To determine the significance of CELSR2 for cell binding and M1 polarization activity of GRS by suppressing the transcript of CELSR2, CELSR2 was suppressed in macrophages with two independent si-RNAs targeting CELSR2 and the binding of biotinylated GRS to RAW264.7 cells was reduced by the

suppression of CELSR2 (Figure 5C,D). In addition, the GRS-dependent induction of TNF-α secretion and transcription was decreased by the suppression of CELSR2 (Figure 5D and 5E). Next, it was checked whether CELSR2 would give any effect on GRS-induced phagocytosis and found that GRS-induced phagocytosis was also lowered by CELSR2 suppression (Figure 5F). All of these results suggest the functional significance of CELSR2 for cell binding and M1 polarization activity of GRS in macrophages.

**M1 polarization activity of GRS effect on tumor growth**

GRS activity was then investigated whether its activity in M1 polarization of macrophages would play any significant role in the control of tumorigenesis. In our previous tumor regression model, GRS specifically suppressed tumor growth of renal carcinoma SN12C cells containing CDH6 receptor, but not RENCA cells lacking functional CDH6 (Park et al., 2012). Since the effect of immune system against tumor formation would be more prominent at the initial stage of tumorigenesis, here it was investigated whether M1 polarization activity of GRS would give any tumor suppressive activity in a tumor initiation model. For this, GRS was treated once a day including the initial day of implantation of SN12C and RENCA cells for a total of 5 days and monitored the tumor growth. It was

observed that both of GRS suppressed the tumor growth regardless of CDH6 while giving little effect on body weight (Figure 6A,B,C,D).

Next, M1 and M2 macrophage infiltration was checked in the isolated tumor tissues and a significant increase of M1 (marked by MHCII staining) and decrease of M2 (marked by CD206 staining) was observed in macrophages in GRS or GRS-EV-treated tumors (Figure 6E). In addition, the tumor tissue treated with GRS showed an increase in apoptosis (Figure 6F).

To give a brief summary of the GRS autocrine effect, a schematic was drawn representing the effect of GRS in tumor microenviroment (Figure 7)

# DISCUSSION

The role of GRS in the M1 polarization of macrophages against tumorigenesis and its secretion carried on extracellular vesicles from macrophages. Although classical M1 type macrophages would work to suppress tumorigenesis, they are tamed by the factors like CSF-1 and IL-10 released from cancer cells(Mantovani et al., 2004a) and polarized to M2 type which would promote tumor growth and mobilization(Sica et al., 2006). Although anti-tumorigenic M1 and pro-tumorigenic M2 type macrophages show different profiles of secreting factors and cellular behavior(Mantovani and Sica, 2010), it is not well understood how the two fates are determined.

This work demonstrated that secreted GRS an important factor for initiating cytokines that skew macrophages toward M1 type in a tumor microenvironment so that macrophages could work against tumor initiation. Based on the results here with our previous finding that GRS is rapidly released from cancer-associated macrophages to directly trigger cancer cell death (Park et al., 2012), GRS appears to exert anti-tumorigenic activity in two distinct routes, namely, via direct apoptotic activity to cancer cells, and also through M1 polarization activity of macrophages. These two activities may work together or work sequentially depending on the context and stage of tumorigenesis.

However not much know about CELSR2 especially regarding the downstream signaling of these receptors. The cadherin super-family is a group of calcium-dependent glycoproteins. Since the first discovery of cadherins in the early 1980's(Hyafil et al., 1981; Peyrieras et al., 1983), the cadherin family has greatly expanded into a superfamily, including classic cadherins (type I and II), protocadherins, desmogleins, desmocollins, and other cadherin-related proteins(Angst et al., 2001). While their functions in cell adhesion and migration, cytoskeletal organization, and morphogenesis have been well studied, their roles in cancer are also rapidly being uncovered(Christofori and Semb, 1999). While GRS was shown to work to cancer cells via CDH6, this work showed its M1 activation of macrophages via CELSR2 that is defined as non-classical seven-pass transmembrane family of cadherin. CELSR2 was also suggested to play a role in protein transport and secretion (Kjolby et al., 2010). The suggested functions of CELSR2 in cell migration and protein secretion appear to support the observed activities of GRS to macrophages although how GRS would activate CELSR2 would require further studies. In this regard, GRS could be used as immunotherapeutic agent against tumorigenesis.

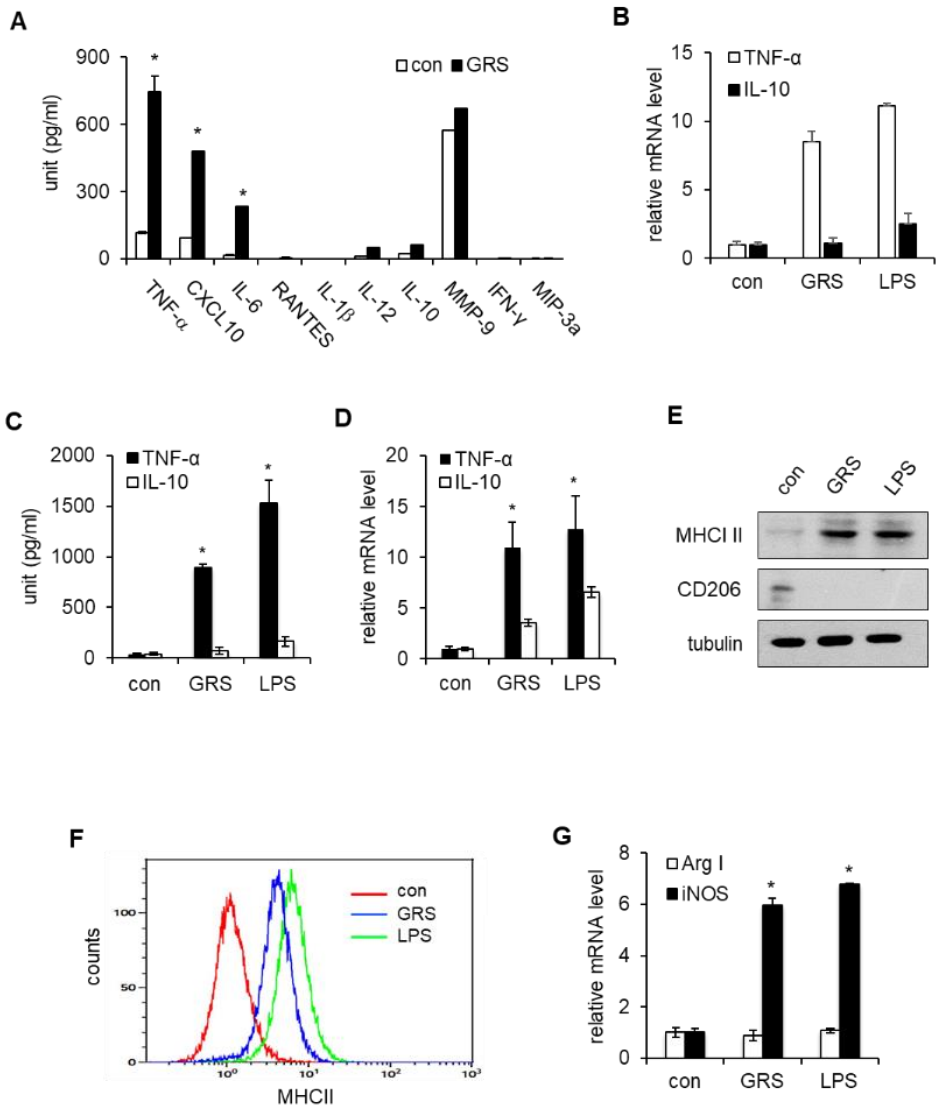


**Figure 1. Secreted GRS induces macrophage M1 polarization**. (A) RAW264.7 cells were treated with GRS (100 nM) for 6 hr. The cultured media were harvested to measure secreted cytokines. Cytokines profiles were determined by multiplex assay, unpaired t test, *P<.0005. (B) RAW264.7 cells were treated with GRS (100 nM) or LPS (50 ng/ml) for 4 hr and the transcript level of TNF-α and IL-10 was determined by qRT-PCR, unpaired t test, *P<.0001. Results are presented in-terms

of a fold change after normalizing with β-actin mRNA, unpaired t test. (C) BMDM cells were subjected to GRS (100 nM) for 6 hours and the secretion of TNF-α and IL-10 was analyzed by ELISA, unpaired t test, *P<.0001. (D) Quantitative PCR (qPCR) analysis of TNF-α and IL-10 mRNA expression in BMDM cells after treatment with GRS (100 nM) for 4 hr, unpaired t test, *P<.0001. Results are presented in-terms of a fold change after normalizing with β-actin. (E) After 24 hr incubation of RAW264.7 cells with GRS and LPS, the M1 and M2 polarization marker proteins, MHCII and CD206, respectively, were determined by immunoblotting (F) RAW264.7 cells were incubated with GRS or LPS for 24 hr and the induction of MHC II was determined by FACS analysis. (G) Quantitative PCR (qPCR) analysis of Arg I and iNOS mRNA expression in RAW cells after treatment with GRS and LPS for 4 hr.

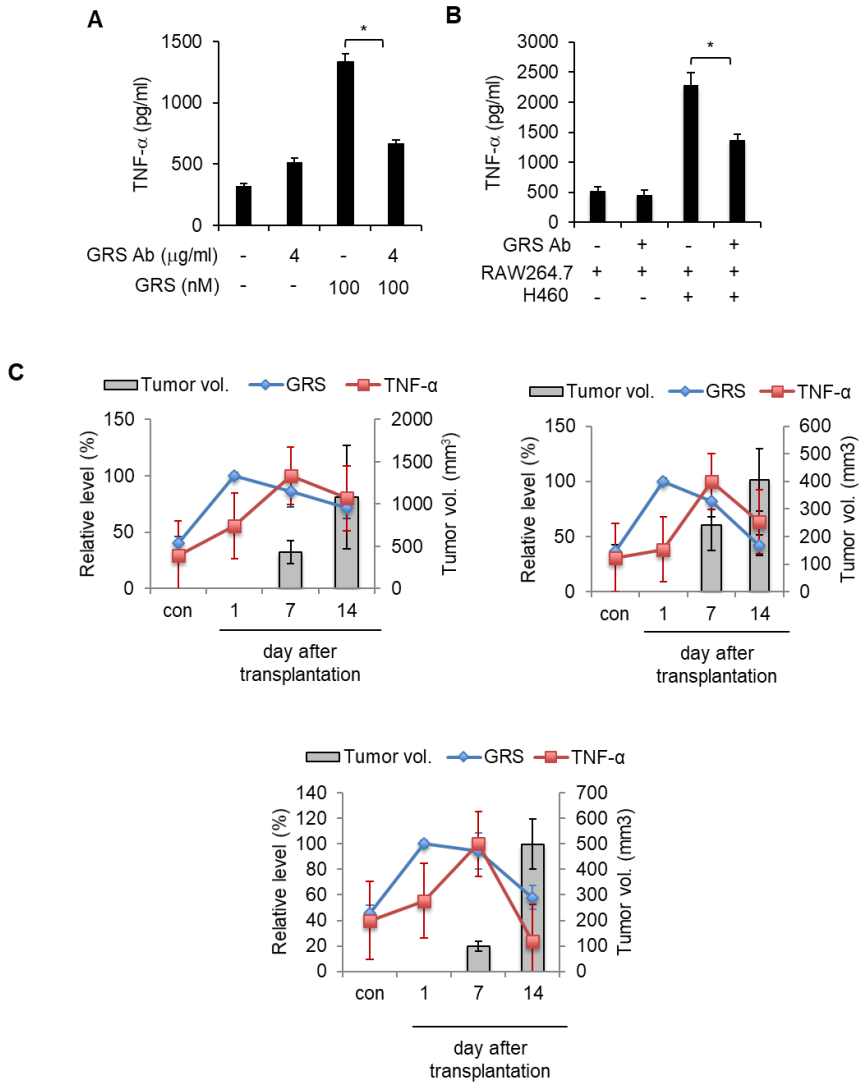


**Figure 2. GRS controls TNF-α secretion in a tumor microenvironment.** (A) GRS alone or GRS pre-incubated with anti-GRS antibody for 30 min and then added to macrophages for 6h. The secreted TNF-α was determined in culture media by ELISA, unpaired t test, *P<.005. (B) Macrophages (RAW264.7) and cancer cells (H460) were co-cultured and then TNF-α secretion was monitored by ELISA. To check GRS effect in co-cultured sample, anti-GRS antibody was added to co-

culture media, unpaired t test, *P<.01. (C) Cancer cells ($5x10^6$) were subcutaneously transplanted into nude mice, and blood was collected on the days indicated. GRS and TNF-α secretion was determined by ELISA. *n*= 6 mice per group.

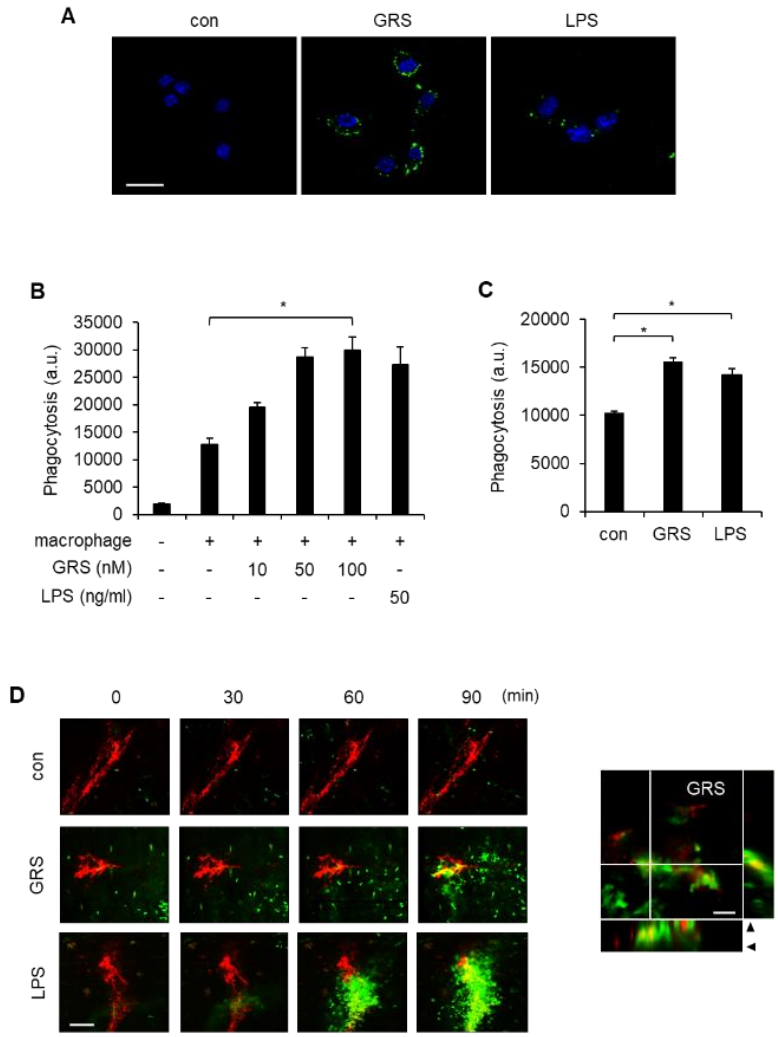


**Figure 3. GRS induces phagocytosis in macrophage** (A)RAW264.7 cells treated with GRS and LPS for 12 hr were incubated with fluorescence-labeled phagocytosis beads (green fluorescence) and the phagocytic activity was monitored

by confocal microscopy. (B) After GRS treatment and LPS as a positive control to RAW264.7 cells, phagocytosis beads were added for 2 hr. To quantify the GRS induced-phagocytosis, the fluorescence intensity was determined by microplate reader. Unpaired t test, *P<.01. (C) BMDM cells were treated with GRS and LPS were treated in the same manner as above, unpaired t test, *P<.01. (D) To determine the effect of GRS and GRS-EVs on phagocytic activity of macrophages in vivo, they were intradermally injected into the ears of LysM-GFP mice. After 6 hr incubation, Alexa594-conjugated particles (red fluorescence) were injected and the movement of macrophage/neutrophil (LysM, green) toward the particles were visualized with custom-built in vivo confocal microscopy for 90 min*. Co-localization of macrophages (green) treated with GRS. Scale bar represents 100 μm (A) and 20 μm (B and C). *Collaboration with Philan Kim

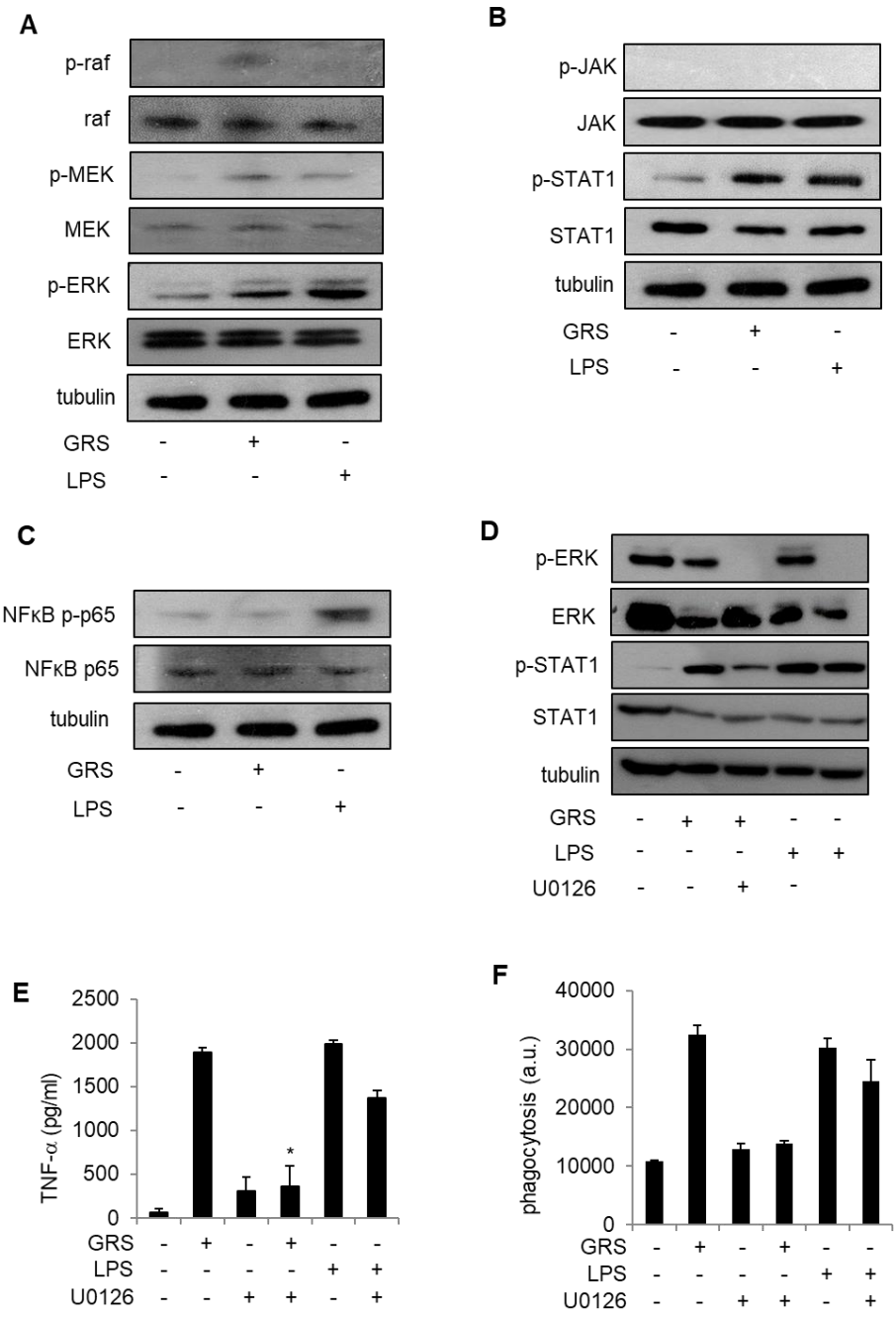
A
p-raf
raf
p-MEK
MEK
p-ERK
ERK
tubulin
GRS - + -
LPS - - +
B
p-JAK
JAK
p-STAT1
STAT1
tubulin
GRS - + -
LPS - - +
C
NFκB p-p65
NFκB p65
tubulin
GRS - + -
LPS - - +
D
p-ERK
ERK
p-STAT1
STAT1
tubulin
GRS - + + - -
LPS - - - + +
U0126 - - + -
E
TNF-α (pg/ml)
2500
2000
1500
1000
500
0
*
GRS - + - + - -
LPS - - - - + +
U0126 - - + + - +
F
phagocytosis (a.u.)
40000
30000
20000
10000
0
GRS - + - + - -
LPS - - - - + +
U0126 - - + + - +

**Figure 4. GRS activity is dependent on RAS-RAF-MEK pathway** (A) RAW 264.7 cells were treated with GRS (100nM) or LPS (50ng) for one hr and the phosphorylation of RAF, MEK and ERK was determined by Western blotting. (B) Cells were subjected to GRS or LPS (50ng) for one hr and the phosphorylation of JAK and STAT1 was shown by immunoblotting (C) Cells were subjected to GRS or LPS (50ng) for one hr and the phosphorylation of NF-κB was shown by western blotting. (D)Cells were pre-treated with MAPK kinase inhibitor, 10 μM U0126 (MEK inhibitor), for 1 hr and then 100 nM GRS or 50ng LPS was added for 1 hr. Their effect on the phosphorylation of ERK and STAT1 was shown by Western blotting. (E) RAW246.7 cells were treated with MEK kinase inhibitor for 1hr and GRS or LPS was treated for 6 hr, the media was collected and the secretion of TNF-α was determined by ELISA, unpaired t test, *P<.0005. (F) MAPK kinase inhibitors 1.25 μM U0126 (MEK inhibitor) was treated to cells and GRS was treated to cells for 12 hr, phagocytosis beads were added for 2 hr. To quantify the GRS induced-phagocytosis, the fluorescence intensity was determined by microplate reader, unpaired t test, *P<.0005.

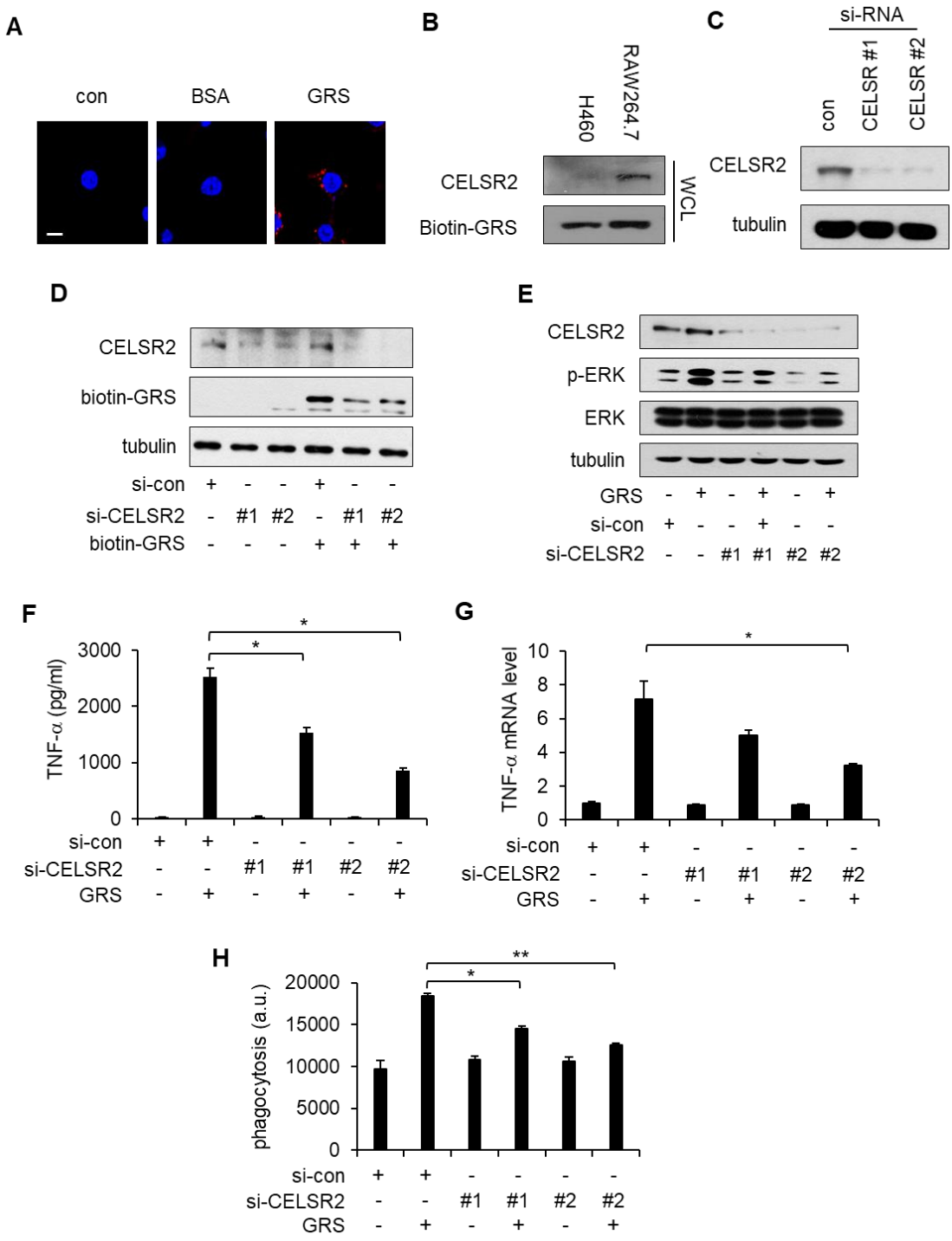
A
con
BSA
GRS
B
H460
RAW264.7
CELSR2
Biotin-GRS
WCL
C
si-RNA
con
CELSR #1
CELSR #2
CELSR2
tubulin
D
CELSR2
biotin-GRS
tubulin
si-con + - - + - -
si-CELSR2 - #1 #2 - #1 #2
biotin-GRS - - - + + +
E
CELSR2
p-ERK
ERK
tubulin
GRS - + - + - +
si-con + - - + - -
si-CELSR2 - - #1 #1 #2 #2
F
TNF-α (pg/ml)
3000
2000
1000
0
si-con + + - - - -
si-CELSR2 - - #1 #1 #2 #2
GRS - + - + - +
G
TNF-α mRNA level
10
8
6
4
2
0
si-con + + - - - -
si-CELSR2 - - #1 #1 #2 #2
GRS - + - + - +
H
phagocytosis (a.u.)
20000
15000
10000
5000
0
si-con + + - - - -
si-CELSR2 - - #1 #1 #2 #2
GRS - + - + - +

**Figure 5. CELSR2 is identified as a receptor for GRS and inhibition reduces GRS binding and M1 activities** (A) RAW 264.7 cells were incubated with Alex-Fluor 647 (red) labeled GRS or BSA (100 nM) for 30 min. Cell nuclei were stained by DAPI (blue) and the images were taken by confocal microscopy. (B) Biotinylated GRS (Biotin-GRS) was incubated with the protein extracts of RAW264.7 and H460 precipitated by streptavidin-sepharose. The GRS-bound proteins were subjected to SDS-PAGE and the presence of endogenous CELSR2 was determined by immunoblotting with its specific antibody. (C) RAW 264.7 cells were transfected with non-specific siRNA (si-con) or two siRNAs targeting the CELSR2 transcript (si-CELSR2 #1, #2). The knockdown of CELSR2 was determined by western blotting. (D) RAW264.7 cells were transfected with non-specific siRNA (si-con) or siRNA targeting the CELSR2 transcript (si-CELSR2), and then incubated with biotin-GRS. (E) RAW 264.7 cells were transfected with two siRNAs targeting the CELSR2 transcript (si-CELSR2 #1, #2) and their effect on the phosphorylation of ERK was determined by Western blotting. (F) RAW264.7 cells transfected with anti-CELSR2 siRNAs as above were treated with GRS (100 nM) for 6 hr and the secretion of TNF-α was analyzed in culture media by ELISA, unpaired t test, *P<.005. (G) Macrophages were treated with si CELSR2 #1, #2 as mentioned above, then cells were incubated with GRS (100 nM) for 4 hr. The TNF-α mRNA level was determined by QPCR normalized to the β-

actin level, unpaired t test, *P<.01. (H) Cells above were also treated with GRS for 12 hr and further incubated with phagocytosis beads (green fluorescence). The phagocytic activity was determined by microplate reader, unpaired t test, *P<.0005, **P<.0001.

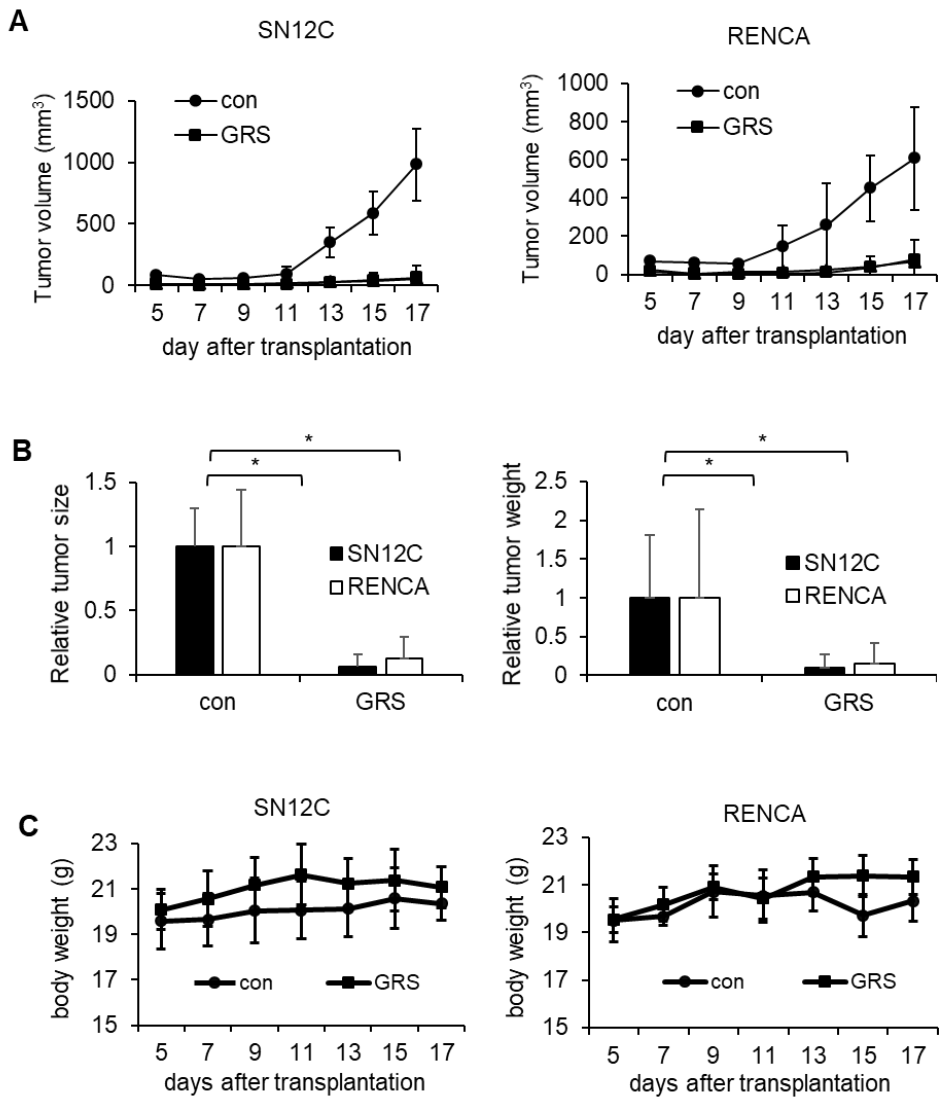
A
SN12C
RENCA
Tumor volume (mm3)
con
GRS
day after transplantation
B
Relative tumor size
Relative tumor weight
SN12C
RENCA
con
GRS
C
body weight (g)
days after transplantation

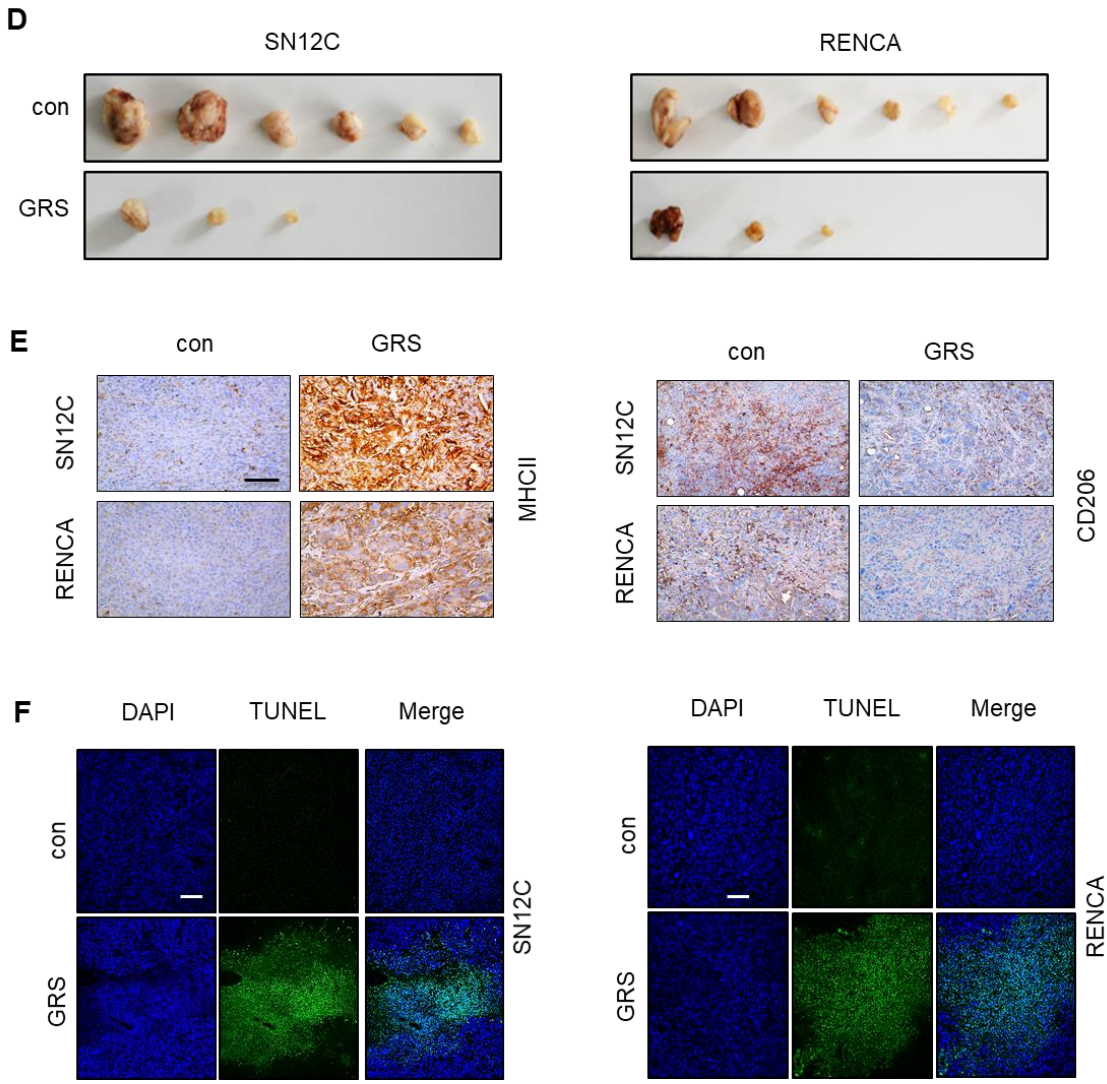


**Figure 6. GRS reduced tumor growth in-vivo initiation model.** The activities of GRS or GRS-EVs against tumor initiation was validated by in vivo xenograft mouse model using renal carcinoma SN12C (CDH6 positive, left panel) and RENCA (CDH6 negative, right panel) cells. The cancer cells (1x107) were subcutaneously transplanted into nude mice, and GRS-EVs (6 mg/kg) and GRS (6

mg/kg) were delivered intraperitoneal injection to mice via once a day for 5 days included initial day of transplantation. n= 6 mice per group. (A) Tumor volumes were measured every 2 days after GRS treatment. (B) Relative size and weights of tumor initiation model (C) Body weights of initiation model were measured; n=3 biological replicates, unpaired t test, *P<.0005. (D) Images of tumor of the tumor initiation model (E) To determine the type of infiltrated macrophages, the tumor tissues treated with GRS and GRS-EVs were stained with anti-MHCII and –CD206 antibodies for immunohistochemistry. Scale bar indicates 100 μm. (F) TUNEL assay staining of the initiation model. Scale bar represents 25 μm.

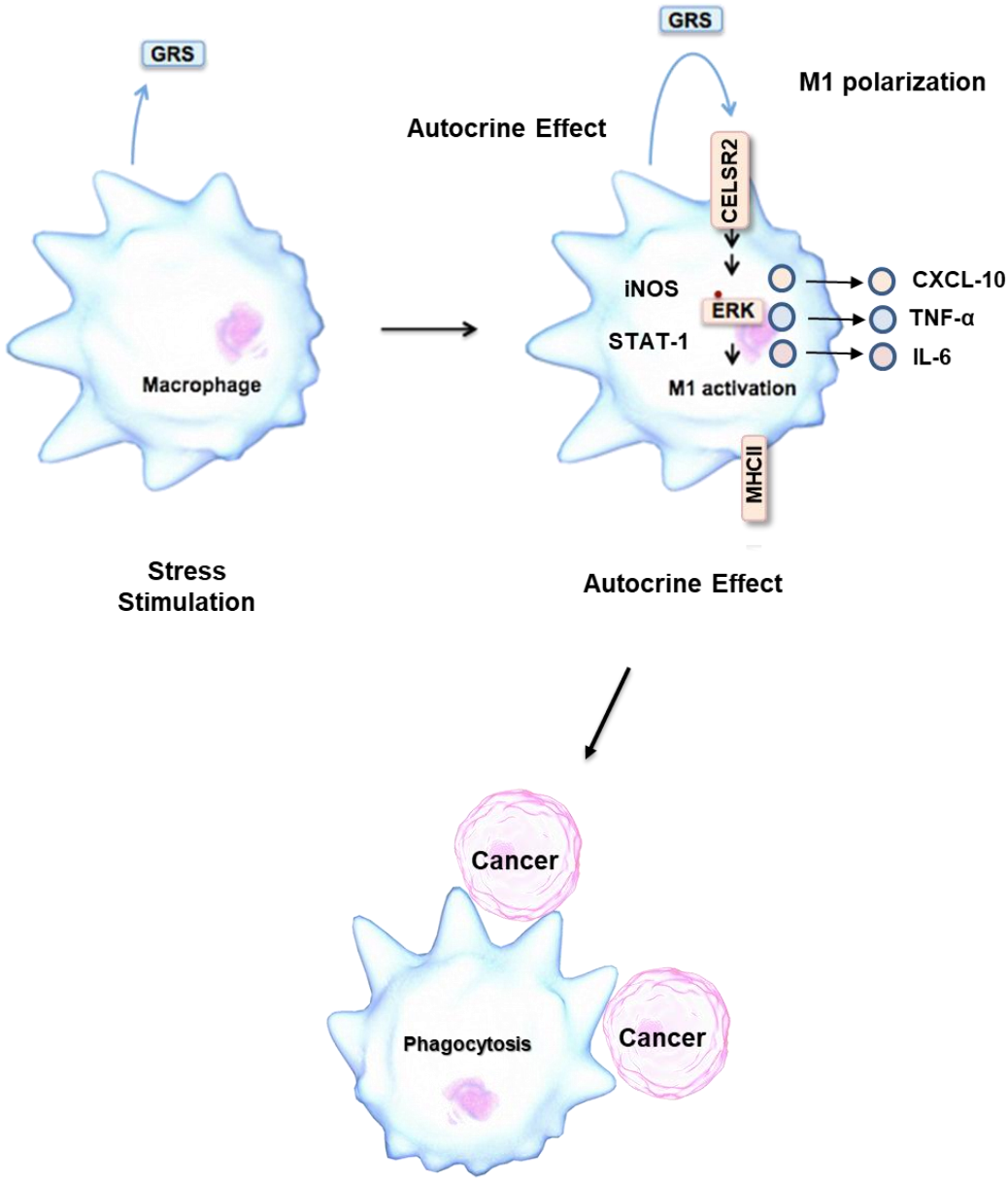


**Figure 7. Schematic representation of the GRS autocrine effect in a tumor microenvironment.**

# MATERIALS AND METHODS

**Cell culture and materials**

RAW264.7 cells were grown in DMEM medium from Hyclone (Logan, UT, USA) containing 10% fetal bovine serum and 50 mg/ml streptomycin and penicillin (Hyclone). Bone marrow derived macrophages (BMDM) were harvested from C57B/6 mice. Bone marrow cells were isolated from femurs and tibias. After red blood cells were removed with ACK solution from Thermo Fisher Scientific (Waltham, MA, USA), bone marrow cells were incubated for 7 days with murine GM-CSF (20 ng/ml) from Peprotech (Rocky Hill, NJ, USA). The antibodies against GRS was purchsed from Neomics (Suwon, Korea), MHC II from Millipore (Billerica, MA, USA), CD206 from Abcam (Cambridge, UK), p-ERK, ERK, p-p38, p38 from Cell Signaling Technology (Danvers, MA, USA) and p-JNK, JNK from Santa Cruz Biotechnology (Dallas, TX, USA). Si-RNAs '5-AUAGGAACCACUCUGGUCAUCUUCC-3′ and '5 AGCAGUAGCCCGUUACGCUCCUUGG-3' targeting CELSR2 were obtained from Invitrogen (Carlsbad, CA, USA). MAPK kinase inhibitors (U0126, SB202190 and SP600125) were purchased from Calbiochem (San Diego, CA, USA).

**Preparation of recombinant human GRS**

Human GRS cDNA encoding 685 amino acids was subcloned into pET-28a (Millipore) with *Eco*RI and *Xho*I, and overexpressed in *Escherichia coli* Rosetta by 0.5 mM IPTG. His-tagged GRS was then purified using nickel affinity chromatography (Invitrogen) following the manufacturer's instruction. To remove lipopolysaccharide (LPS), the purified protein solution was dialyzed in pyrogen-free potassium buffered saline (PBS, pH 7.4) containing 15% glycerol. After dialysis, the GRS-containing solution was filtered through Acrodisc unit with Mustang E membrane from Pall Corporation (Port Washington, NY, USA). Endotoxin was measured by limulus amebocyte lysate (LAL) assay from Pierce (Rockford, IL, USA). Recombinant GRS protein contained endotoxin less than 1 EU/ml.

**Cell binding assay**

RAW264.7 cells were seeded into six-well dishes and incubated for 12 hr. Then, the biotinylated GRS was added to the culture medium and further incubated for the indicated times. The cells were washed 4 times with cold PBS and then lysed in

25 mM Tris-HCl (pH 7.4) lysis buffer containing 150 mM NaCl, 2 mM EDTA, 1% Triton X-100, 1% sodium deoxycholate, 10 mM NaF, 1 mM sodium orthovanadate, 10% glycerol and protease inhibitors and centrifuged at 18,000 *g* for 15 min. The extracted proteins were resolved by SDS/PAGE, and detected by streptavidin-coupled HRP (Pierce). For biotinylation, recombinant GRS (1.5 mg) was incubated with 0.25 mg sulfo-NHS-SS-biotin (Pierce) in PBS for 2.5 hr at 4°C. Free biotins were quenched with glycine and removed by size exclusion column, PD10 from GE Healthcare (Chicago, IL, USA). To monitor cell binding of GRS by immunofluorescence staining, BSA and GRS were labeled with Alexa-Fluor 647 (Life technologies). RAW cells were then seeded on 22 x 22 mm coverslips. Labeled BSA (100 nM) or GRS (100 nM) was added to the media for 30 min. Next the cells were washed with cold PBS two times. The cells were fixed with 4% formaldehyde from Affymetrix (Santa Clara, CA, USA) for 10 minutes, washed two times, and then stained with DAPI (Life technologies) for 10 min and washed three times and mounted on the microscope slide. The cells were mounted and observed by confocal microscopy (Nikon A1, Tokyo, Japan).

**Immunofluorescence**

RAW264.7 cells were seeded on 22 x 22 mm cover glass. The conditioned cells were washed twice by PBS and then fixed with 4% paraformaldehyde for 10 min.

The samples were blocked by CAS-block™ (Thermo Scientific) for 30 min and then incubated with anti-GRS antibody for 2 hr. Anti-GRS antibody was captured with Alexa488-conjugated secondary antibody (Thermo Scientific). Nuclei were stained with DAPI (4',6-diamidino-2-phenylindole, Invitrogen). ER and Lyso tracker (Thermo Scientific) were used to stain intracellular endoplasmic reticulum and lysosomes, respectively. Before fixation, each tracker was incubated with the cells for 2 hr and visualized by confocal microscopy-A1R (Nikon).

**Flow cytometry analysis**

RAW264.7 cells were first incubated in staining buffer (PBS with 2% fetal calf serum and 0.1% $NaN_3$) containing hamster and mouse IgGs from PharMingen (San Diego, CA, USA) for 15 min on ice to block non-specific binding. The cells were then stained with MHC class II antibody for 45 min on ice and analyzed by FACScan using CellQuest software (BD Biosciences).

**Phagocytosis assay**

Macrophage phagocytic activity was measured using the Vybrant Phagocytosis Assay Kit (Thermo Fisher Scientific). Briefly, RAW264.7 cells were seeded in a 96-well plate. The cells were treated with GRS (100 nM) and LPS (50 ng/ml) for 12 hr. After treatment, the cells were further incubated with fluorescein-labeled phagocytosis beads for 2 hr, which after extracellular fluorescence was quenched

by trypan blue, and phagocytic activity was quantified by measuring fluorescence intensity using microplate reader (BMG Labtech FLUOstar OPTIMA, Ortenberg, Germany). For immunofluorescence phagocytosis assay, RAW264.7 cells were seeded on coverslips for 12 hr and serum starved for 2 hr. BSA (100 nM), GRS (100 nM) or LPS (50 ng/mL) was added to the media for 12 hr. The cells were fixed with 4% formaldehyde for 10 min, and then permeabilized with 0.1% Triton-X in PBS for 5 min. The cells were then incubated with E.Coli (K12)-alexa fluor-488 bioparticle (Thermo Fisher Scientific) for 10 min and washed two times, then stained with DAPI from Molecular Probes (Eugene, OR, USA) for 10 min and washed three times and mounted. The images were taken with confocal microscopy (Nikon A-1).

**ELISA and multiplex assay**

RAW264.7 cells were cultured in 12 well plates. Different amounts of GRS were added to the media. After 6 hr incubation, the media was collected and spun down by centrifugation at 3,000 *g* for 10 min. The secreted TNF-α and IL-10 were detected using the ELISA kit following manufacturer's instruction (BD Biosciences, San Jose, CA, USA). The cytokine level of samples was measured by microplate reader (TECAN, Mannedorf, Swiss). For multiplex assay, TNF-α, IL-6, RANTES, IL-1β, IL-12, IL-10, MMP-9, INF-γ, MIP-3α and CXCL10 premixed

beads were purchased from R&D Science (Minneapolis, MN, USA). Standards and samples were incubated with the beads on plate shaker for 2hr. Second antibody was added to each well. After 1 hr incubation, streptavidn-PE solution was added and further incubated for 30 min. The beads were measured with luminex system (BioRad, Bioplex 200, Hercules, CA, USA) and analyzed by bioplex software (BioRad 6.0).

**qRT-PCR assay**

Cells were incubated on six-well dishes for 12 hr and then stimulated with His-GRS (100 nM) for indicated times. Total RNAs were extracted by using RNeasy mini kit from QIAGEN (Germantown, MD, USA). cDNA was synthesized using maxima first strand cDNA synthesis kit (Thermo Fisher Scientific). qRT-PCR was performed with the primers specific to the TNF-α, IL-10, iNOS, Arg-I and β-actin.

TNF-α: 5'-CTCAAAATTCGAGTGACAAGCCTG-3'(forward),

5'-ATCGGCTGGCACCACTAGTT-3'(reverse),

IL-10: 5'-AGACTTTCTTTCAAACAAAGGA-3'(forward),

5'- ATCGATGACAGCGCCTCAG-3'(reverse),

iNOS: 5'- CAGCTGGGCTGTACAAACCTT-3'(forward),

5'-CATTGGAAGTGAAGCGTTTCG-3'(reverse),

Arg-I: 5’- AAGAAAAGGCCGATTCACCT-3’ (forward),

5’-CACCTCCTCTGCTGTCTTCC-3’ (reverse),

β-actin: 5’-GGCTGTATTCCCCTCCATCG-3’ (forward),

5’- CCAGTTGGTAACAATGCCAT -3’. To calculate the quantitative RNA level, samples were analyzed by Maxima SYBR Green/ROX qPCR master mix (Thermo Fisher Scientific) on Thermal Cycler Dice™ Real Time system (Takara, Shiga, Japan) according to manufacturer’s protocols. β-actin mRNA levels were used as internal controls.

***In vivo* tumor model**

Xenograft experiments were performed in accordance with the University Animal Care and Use Committee guidelines at Seoul National University. For the initiation model, SN12C and RENCA cells ($1 \times 10^7$) were injected subcutaneouly into the right flank of 8-week-old BALB/c female nude mice. Tumor volume was measured as length x width$^2$ x 0.5 using caliper. The purified GRS and GRS-EVs were administrated by intraperitoneal injection in a single dosage of 6 mg/kg/day for 5 days including the initial day of xenograft. Tumor weights and sizes were measured on the day of sacrifice.

**Intravital phagocytosis imaging**

The *in vivo* effect of GRS on phagocytic activity of macrophages was monitored by custom-built laser-scanning confocal microscopy. To implement 2D scanning, fastrotating polygonal mirror (Lincoln Laser, Phoenix, AZ, USA) and galvanometer (Cambridge Technology, Cambridge, MA, USA) were used. High-sensitive photomultiplier tubes (Hamamatsu Photonics, Hamamatsu, Japan) were utilized to detect three-color fluorescence signals simultaneously. Three detection channels were split by dichroic mirrors and bandpass filters (Semrock, Rochester, NY, USA). Electric signals obtained from PMT were digitized by an 8-bit 3-channel frame grabber (Matrox, Dorval, Canada). After acquired from the imaging system, 512x512 pixel images were then XY-shift compensated with Matlab (Mathworks, Natick, MA, USA) and reconstructed on either XZ/YZ axis by ImageJ software. For intravital phagocytosis imaging, the male LysM-GFP (Lysozyme M-GFP) mice (18-22 week old) were used. Mice were anaesthetized with mixture of Zoletil (30 mg/kg, Virbac, Carros, France) and xylazine (10 mg/kg, Bayer-Korea, Seoul, Korea). Alexa-405 (Thermo Fisher Scientific)-conjugated GRS (1 μg) was intradermally injected into mouse ear skin with 31G micro-injector Hamilton syringe (Sigma-Aldrich). After 6 hr incubation, E.Coli (K12)-Alexa fluor-594 bioparticle (Thermo Fisher Scientific) were injected at GRS

injection sites and phagocytosis was visualized with confocal microscopy platform for 90 min.

**Immunohistochemistry**

The isolated tumors were stored in 4% formaldehyde from Junsei Chemical (Tokyo, Japan) for 24 hr. The tumor tissues were parafilmed blocked and sectioned to 10 µm by WooJung BSC (Osong, South Korea). The sections were incubated with anti-MHCII antibody (Millipore) or anti-CD206 (Abcam) and visualized with anti-mouse HRP conjugated antibody from Dako (Carpinteria, CA, USA) and DAB substrate (Dako). After visualization, the slides were counterstained with hematoxylin (Sigma-Aldrich). Immunohistochemical staining was analyzed by Optinity microscope (Lieca) with Toupview program.

**Data analysis**

Statistical Analysis Results from multiplex beads, phagocytosis, ELISA and qPCR data were presented as mean ± standard deviation. Statistical significance was computed with Microsoft Excel 2016 unpaired Student's t test with a p value of $< 0.05$ considered as significant.

# REFERENCES

Ahn, Y.H., Park, S., Choi, J.J., Park, B.K., Rhee, K.H., Kang, E., Ahn, S., Lee, C.H., Lee, J.S., Inn, K.S., *et al.* (2016). Secreted tryptophanyl-tRNA synthetase as a primary defence system against infection. Nat. Microbiol. *2*, 16191.

Angst, B.D., Marcozzi, C., and Magee, A.I. (2001). The cadherin superfamily: diversity in form and function. J. Cell Sci. *114*, 629-641.

Bakos, E., Evers, R., Sinko, E., Varadi, A., Borst, P., and Sarkadi, B. (2000). Interactions of the human multidrug resistance proteins MRP1 and MRP2 with organic anions. Mol. Pharmacol. *57*, 760-768.

Bobrie, A., Colombo, M., Krumeich, S., Raposo, G., and Thery, C. (2012). Diverse subpopulations of vesicles secreted by different intracellular mechanisms are present in exosome preparations obtained by differential ultracentrifugation. J. Extracell. Vesicles *1*.

Choe, K., Hwang, Y., Seo, H., and Kim, P. (2013). In vivo high spatiotemporal resolution visualization of circulating T lymphocytes in high endothelial venules of lymph nodes. J. Biomed. Opt. *18*, 036005.

Christofori, G., and Semb, H. (1999). The role of the cell-adhesion molecule E-cadherin as a tumour-suppressor gene. Trends Biochem. Sci. *24*, 73-76.

Cocucci, E., Racchetti, G., and Meldolesi, J. (2009). Shedding microvesicles: artefacts no more. Trends Cell Biol. *19*, 43-51.

Faust, N., Varas, F., Kelly, L.M., Heck, S., and Graf, T. (2000). Insertion of enhanced green fluorescent protein into the lysozyme gene creates mice with green fluorescent granulocytes and macrophages. Blood *96*, 719-726.

Fujiwara, T., Oda, K., Yokota, S., Takatsuki, A., and Ikehara, Y. (1988). Brefeldin A causes disassembly of the Golgi complex and accumulation of secretory proteins in the endoplasmic reticulum. J. Biol. Chem. *263*, 18545-18552.

Gajewski, T.F., Schreiber, H., and Fu, Y.-X. (2013). Innate and adaptive immune cells in the tumor microenvironment. Nat. Immunol. *14*, 1014-1022.

Gordon, S., and Martinez, F.O. (2010). Alternative Activation of Macrophages: Mechanism and Functions. Immunity *32*, 593-604.

Gudz, T.I., Tserng, K.Y., and Hoppel, C.L. (1997). Direct inhibition of mitochondrial respiratory chain complex III by cell-permeable ceramide. J. Biol. Chem. *272*, 24154-24158.

Hirayama, A., Kami, K., Sugimoto, M., Sugawara, M., Toki, N., Onozuka, H., Kinoshita, T., Saito, N., Ochiai, A., Tomita, M.*, et al.* (2009). Quantitative Metabolome Profiling of Colon and Stomach Cancer Microenvironment by Capillary Electrophoresis Time-of-Flight Mass Spectrometry. Cancer Res. *69*, 4918-4925.

Hyafil, F., Babinet, C., and Jacob, F. (1981). Cell-cell interactions in early embryogenesis: a molecular approach to the role of calcium. Cell *26*, 447-454.

Jun, S., Ke, D., Debiec, K., Zhao, G., Meng, X., Ambrose, Z., Gibson, G.A., Watkins, S.C., and Zhang, P. (2011). Direct visualization of HIV-1 with correlative

live-cell microscopy and cryo-electron tomography. Structure *19*, 1573-1581.

Kjolby, M., Andersen, O.M., Breiderhoff, T., Fjorback, A.W., Pedersen, K.M., Madsen, P., Jansen, P., Heeren, J., Willnow, T.E., and Nykjaer, A. (2010). Sort1, encoded by the cardiovascular risk locus 1p13.3, is a regulator of hepatic lipoprotein export. Cell Metab. *12*, 213-223.

Lee, H.S., Bae, T., Lee, J.H., Kim, D.G., Oh, Y.S., Jang, Y., Kim, J.T., Lee, J.J., Innocenti, A., Supuran, C.T.*, et al.* (2012). Rational drug repositioning guided by an integrated pharmacological network of protein, disease and drug. BMC Syst. Biol. *6*, 80.

Luga, V., Zhang, L., Viloria-Petit, A.M., Ogunjimi, A.A., Inanlou, M.R., Chiu, E., Buchanan, M., Hosein, A.N., Basik, M., and Wrana, J.L. (2012). Exosomes mediate stromal mobilization of autocrine Wnt-PCP signaling in breast cancer cell migration. Cell *151*, 1542-1556.

Mantovani, A., and Sica, A. (2010). Macrophages, innate immunity and cancer: balance, tolerance, and diversity. Curr. Opin. Immunol. *22*, 231-237.

Mantovani, A., Sica, A., Sozzani, S., Allavena, P., Vecchi, A., and Locati, M. (2004a). The chemokine system in diverse forms of macrophage activation and polarization. Trends Immunol. *25*, 677-686.

Mantovani, A., Sica, A., Sozzani, S., Allavena, P., Vecchi, A., and Locati, M. (2004b). The chemokine system in diverse forms of macrophage activation and polarization. Trends Immunol. *25*, 677-686.

Mathivanan, S., and Simpson, R.J. (2009). ExoCarta: A compendium of exosomal

proteins and RNA. Proteomics *9*, 4997-5000.

Means, T.K., Pavlovich, R.P., Roca, D., Vermeulen, M.W., and Fenton, M.J. (2000). Activation of TNF-alpha transcription utilizes distinct MAP kinase pathways in different macrophage populations. J. Leukoc. Biol. *67*, 885-893.

Milligan, G., Parenti, M., and Magee, A.I. (1995). The dynamic role of palmitoylation in signal transduction. Trends Biochem. Sci. *20*, 181-187.

Mosmann, T.R., and Coffman, R.L. (1989). TH1 and TH2 cells: different patterns of lymphokine secretion lead to different functional properties. Annu. Rev. Immunol. *7*, 145-173.

Movahedi, K., Laoui, D., Gysemans, C., Baeten, M., Stange, G., Van den Bossche, J., Mack, M., Pipeleers, D., In't Veld, P., De Baetselier, P., and Van Ginderachter, J.A. (2010). Different tumor microenvironments contain functionally distinct subsets of macrophages derived from Ly6C(high) monocytes. Cancer Res. *70*, 5728-5739.

Nickel, W., and Seedorf, M. (2008). Unconventional mechanisms of protein transport to the cell surface of eukaryotic cells. Annu. Rev. Cell Dev. Biol. *24*, 287-308.

Ohno, S., Takanashi, M., Sudo, K., Ueda, S., Ishikawa, A., Matsuyama, N., Fujita, K., Mizutani, T., Ohgi, T., Ochiya, T.*, et al.* (2013). Systemically injected exosomes targeted to EGFR deliver antitumor microRNA to breast cancer cells. Mol. Ther. *21*, 185-191.

Ohtani, Y., Irie, T., Uekama, K., Fukunaga, K., and Pitha, J. (1989). Differential

effects of alpha-, beta- and gamma-cyclodextrins on human erythrocytes. FEBS J. *186*, 17-22.

Park, M.C., Kang, T., Jin, D., Han, J.M., Kim, S.B., Park, Y.J., Cho, K., Park, Y.W., Guo, M., He, W.*, et al.* (2012). Secreted human glycyl-tRNA synthetase implicated in defense against ERK-activated tumorigenesis. Proc. Natl. Acad. Sci. USA *109*, E640-647.

Pece, S., and Gutkind, J.S. (2000). Signaling from E-cadherins to the MAPK pathway by the recruitment and activation of epidermal growth factor receptors upon cell-cell contact formation. J. Biol. Chem. *275*, 41227-41233.

Peters, L.R., and Raghavan, M. (2011). Endoplasmic reticulum calcium depletion impacts chaperone secretion, innate immunity, and phagocytic uptake of cells. J. Immunol. *187*, 919-931.

Peyrieras, N., Hyafil, F., Louvard, D., Ploegh, H.L., and Jacob, F. (1983). Uvomorulin: a nonintegral membrane protein of early mouse embryo. Proc. Natl. Acad. Sci. USA *80*, 6274-6277.

Raposo, G., and Stoorvogel, W. (2013). Extracellular vesicles: exosomes, microvesicles, and friends. J. Cell Biol. *200*, 373-383.

Saccani, A., Schioppa, T., Porta, C., Biswas, S.K., Nebuloni, M., Vago, L., Bottazzi, B., Colombo, M.P., Mantovani, A., and Sica, A. (2006). p50 nuclear factor-kappaB overexpression in tumor-associated macrophages inhibits M1 inflammatory responses and antitumor resistance. Cancer Res. *66*, 11432-11440.

Shaw, R.J. (2006). Glucose metabolism and cancer. Curr. Opin. Cell Biol. *18*, 598-608.

Sica, A., and Mantovani, A. (2012). Macrophage plasticity and polarization: in vivo veritas. J. Clin. Invest. *122*, 787-795.

Sica, A., Schioppa, T., Mantovani, A., and Allavena, P. (2006). Tumour-associated macrophages are a distinct M2 polarised population promoting tumour progression: potential targets of anti-cancer therapy. Eur. J. Cancer (Oxford, England : 1990) *42*, 717-727.

Skog, J., Wurdinger, T., van Rijn, S., Meijer, D.H., Gainche, L., Sena-Esteves, M., Curry, W.T., Jr., Carter, B.S., Krichevsky, A.M., and Breakefield, X.O. (2008). Glioblastoma microvesicles transport RNA and proteins that promote tumour growth and provide diagnostic biomarkers. Nat. Cell Biol. *10*, 1470-1476.

Thery, C., Zitvogel, L., and Amigorena, S. (2002). Exosomes: composition, biogenesis and function. Nat. Rev. Immunol. *2*, 569-579.

Uehata, M., Ishizaki, T., Satoh, H., Ono, T., Kawahara, T., Morishita, T., Tamakawa, H., Yamagami, K., Inui, J., Maekawa, M., and Narumiya, S. (1997). Calcium sensitization of smooth muscle mediated by a Rho-associated protein kinase in hypertension. Nature *389*, 990-994.

Usui, T., Shima, Y., Shimada, Y., Hirano, S., Burgess, R.W., Schwarz, T.L., Takeichi, M., and Uemura, T. (1999). Flamingo, a seven-pass transmembrane cadherin, regulates planar cell polarity under the control of Frizzled. Cell *98*, 585-595.

Valadi, H., Ekstrom, K., Bossios, A., Sjostrand, M., Lee, J.J., and Lotvall, J.O. (2007). Exosome-mediated transfer of mRNAs and microRNAs is a novel mechanism of genetic exchange between cells. Nat. Cell Biol. *9*, 654-659.

Wakasugi, K., and Schimmel, P. (1999). Two Distinct Cytokines Released from a Human Aminoacyl-tRNA Synthetase. Science *284*, 147-151.

Wakasugi, K., Slike, B.M., Hood, J., Otani, A., Ewalt, K.L., Friedlander, M., Cheresh, D.A., and Schimmel, P. (2002). A human aminoacyl-tRNA synthetase as a regulator of angiogenesis. Proc. Natl. Acad. Sci. USA *99*, 173-177.

Xin, H., Li, Y., Cui, Y., Yang, J.J., Zhang, Z.G., and Chopp, M. (2013). Systemic administration of exosomes released from mesenchymal stromal cells promote functional recovery and neurovascular plasticity after stroke in rats. J. Cereb. Blood Flow Metab. *33*, 1711-1715.

Ziegler-Heitbrock, H.W., Fingerle, G., Strobel, M., Schraut, W., Stelter, F., Schutt, C., Passlick, B., and Pforte, A. (1993). The novel subset of CD14+/CD16+ blood monocytes exhibits features of tissue macrophages. Eur. J. Immunol. *23*, 2053-2058.

Zitvogel, L., Regnault, A., Lozier, A., Wolfers, J., Flament, C., Tenza, D., Ricciardi-Castagnoli, P., Raposo, G., and Amigorena, S. (1998). Eradication of established murine tumors using a novel cell-free vaccine: dendritic cell-derived exosomes. Nat. Med. *4*, 594-600.

# CHAPTER 2

# Development of Glycyl-tRNA Synthetase Derived Peptides with Anti-cancer Activity

**Keywords** : Glycyl-tRNA Synthetase, Cancer, Cadherin-6, Peptide, Therapeutic drug, Cadherin-6

# INTRODUCTION

Recently peptides have been the focus of drug development. They are more selective to their target because of more interaction sites than small molecules making them highly selective and more efficacious. Also peptides have less side effects, so they are well tolerated and safe. Consequently, there is an increased interest in peptides in pharmaceutical research and development (R&D), and approximately 140 peptide therapeutics are currently being evaluated in clinical trials. The peptide drugs make up around 10% of the pharmaceutical market.

An array of proteins are in an inactive forms in our bodies. They have to be cleaved to expose their active site. Prepoinsulin is a zymogen, an inactive protein, needs to be cleaved to be active to be change to its active form called insulin. It has been shown that Aminoacyl-tRNA Synthetases (ARSs) are cleaved are cleaved as well forming shorter peptides that have a different role than the full length. For instance, Tyrosyl-tRNA Synthetase (YRS) is cleaved to generate two peptides with distinct activities. N-terminal Tryptophanyl-tRNA Synthetase (WRS), designated mini-WRS is secreted to suppress angiogenesis.

The cadherin superfamily is divided into five subfamilies: cadherins; desmosomal cadherins; protocadherins; fat-like cadherins and flamingo cadherins

Cadherins are important for cell to cell binding but there have been reports for their association to cancer growth and metastasis. The loss of epithelial cadherin (E-cadherin) is associated with poor prognosis and metastatic diseases, which is important to maintain epithelial cells' structure. Cadherin 6 (CDH6), classical type II cadherin with extracellular repeats has been shown to have a role in thyroid, ovarian and renal cancer. It is highly expressed in the kidney, so it is given the kidney cadherin (K-Cadherin).

It was previously reported that GRS specifically binds to CDH6. Cleaving GRS different domains can give insight to where its active site is found. This could lead to a novel therapy for kidney cancer since there is no medication currently used directly to treat renal cancer.

In this study, I found at active region of GRS and developed a peptide that binds to CDH6 inducing apoptosis. By using modeling the binding sites were determined and validated by in-vitro screening. Different lengths of peptide were tested in-vivo through different injection methods. The xenograft mouse model having tumor suppressing effect toward CDH6-positive cell line only. By making a cyclic peptide increased the stability to make a great drug candidate.

# RESULTS

**GRS derived fragment 4(F4) induces tumor regression by binding to CDH6**

To analyze which region of GRS has activity against tumor growth, four fragments of GRS were cut and cloned without interfering with the WHEP, catalytic and anti-codon binding domains of GRS(Fig. 1A-B). GRS fragments were purified and their binding to CDH6 was tested by pull-down assay. Fragment 4 (F4) was the only protein that showed CDH6 binding.(Fig. 1C). Four fragments were tested for anti-tumor effect on cell lines SN12C, MCF-7 and RAW264.7 cell lines. The fragments had no cytotoxic effect on RAW264.7 or MCF-7 cells, CDH6 negative cell lines. However, F4 did show cell killing effect toward SN12C, CDH6 positive cell line (Fig. 1D).. Based on this data the effect of F4 was further investigated

**N-terminal region of F4 is critical for anti-tumor activity**

Due to seeing anti-cancer effect from F4, N-terminal region was truncated in order to reduce non-specific binding and conformation changes in F4. Because GRS N-terminal has beta sheet and inserted into the inner area of GRS, three different N-terminal truncated forms of F4 were designed. Using three different

length of N-terminal truncated form of F4s (for convenience, GRS-F4-N-terminal truncated formed was names GRS-F4-NT) were designed based on the structure, minimizing the conformation changes and retaining alpha and beta sheet in structure (Fig. 2A). The yield, anti-tumor activity of GRS, F4, GRS-F4-NT1, GRS-F4-NT2, and GRS-F4-NT3 were measured to see which form of F4s is suitable to use to find CDH6 binding domain (Fig. 2B). When the N-terminal regions were truncated, the activity of F4 fragments decreased. Analysis of N-terminal truncated form of F4 on the anti-tumor activity gave a clue on the CDH6 binding site, which may locate from 526 residue to 558 residue. These results suggest that F4 is suitable for finding CDH6 binding domain.

**Structure-based docking model predicts the binding site of F4 and CDH6**

F4 and CDH6 structure was used from Protein Data Bank (PDB) and the potential interaction domain of CDH6/F4 complex were predicted using the protein-protein docking software HADDOCK2.2. Based on the model run by the program, six residues were selected and point-mutated using opposite trend of amino acid (Fig. 3A). Residues containing arginine, the key of binding (a hotspot residue), was changed to alanine, which has negatively affected in binding. For F539, phenylalanine was mutated into glutamic acid giving negative charge to

interrupt the binding. Each mutant was purified and checked for the purity using Coomassie staining (Fig. 3B). CDH6 binding activity of F4 mutants were measured using ELISA having GRS used as control. Comparing to F4, F539E and E609A mutants had decreased in CDH6 binding activity and also showed decreased anti-tumor activity (Fig. 3C-D).

**Confirming active site domain using stringent mutation.**

The nearby residues were point-mutated into stringent mutant to increase the disruption in binding with CDH6 for determining the effect on binding and activity. In order to avoid structure conformational changes, stringent mutation was introduced in alpha helix structure and also outer part of F4. Tyrosine, phenylalanine and asparagine were mutated into glutamate or arginine for swapping the charges. Serine was also mutated into tryptophan to introduce bulky amino acid for disrupting the interface (Fig. 4A). Mutated F4 was purified before the experiment checking protein purity through Coomassie staining (Fig. 4B). Using ELISA having GRS as control, F535E showed dramatic decrease in binding and S568W and N570R also showed decrease in CDH6 binding activity (Fig. 4C). F535E residue showed no anti-tumor effects and S568W and N570R residues showed low cancer killing effect (Fig. 4D). Dramatic decrease in binding and anti-tumor activities was observed by introducing stringent mutation in binding domain

area. These results suggest that F535 residue, along with S568 and N570 residues are involved in the CDH6 binding site.

**Double point mutation showing critical interaction between F4 and CDH6**

F535, S568 and N570 residues were used for double point mutation. Structure model showed binding area could be divided into two areas 532 to 549 and 568 to 597. To increase binding disruption, each area was double point mutated including F535, S568 and N570 residues (Fig. 5A). Double mutants and F4 were purified and purity of proteins was checked through coomassie staining (Fig. 5B). ELISA was used to check for CDH6 binding and double mutants having F535 (B-4 and B-5) showed dramatic decrease in binding and mutants with S568 and N570 (A-1) also showed decreased in binding with CDH6 (Fig. 5C). Pull-down assay was performed in order to confirm CDH6 binding. A-1, B-4 and B-5 mutants showed same result with ELISA confirming that mutants associated with F535 and S548/N570 mutants showed dramatic decrease in binding when compared to F4 (Fig. 5D). A-1, B-4 and B-5 showed no anti-cancer effect showing that loss of binding with CDH6 could not induce anti-tumor effect (Fig. 5E).

**CDH6 binding and anti-tumor effects of peptide designed based on stringent mutant model**

A peptide was next designed to include all six residues identified from stringent mutation studies about the CDH6 binding domain. Peptide also has alpha-helix on both ends to retain stability and conformation having two beta-sheets (Fig. 6A). Peptide showed 80% of the CDH6 binding activity when compared to GRS (Fig. 6B). To see CDH6-dependent activity of peptide, CDH6 and pERK positive and negative cell lines were tested. Only CDH6 positive cell lines showed decrease in cell viability (Fig. 6C). CDH6 positive and negative renal cancer cell line was used to see peptide dose-dependent activity. Peptide showed activity toward CDH6 expressing cell line, SN12C, in dose-dependent manner (Fig. 6D). To see if the peptide dephosphorylates ERK through CDH6 binding, CDH6 positive cell line, SN12C and negative cell line, RENCA, were used to check dephosphorylation of ERK (Fig. 6E-F). The melting temperature(Tm) was measured using thermal shift assay and peptide showed 53.44°C in melting temperature (Fig. 6G). Thus, it was found that GRS-derived peptide induces cancer cell death through dephosphorylation of ERK in CDH6 dependent manner.

**Peptide induces tumor regression in CDH6 positive cancer cell *in vivo* not in CDH6 negative cancer cell**

To investigate the peptide effect toward CDH6-positive cell line *in vivo*, peptides were tested in xenograft mouse model using SN12C cells and RENCA

cells. CDH6-positive cell line, SN12C, and CDH6-negative cell line were injected into Balb/c nude mice, and tumors were grown until the average size reaches $100mm^3$. On day 7 and day 9, PBS and 20 μg of GRS and peptide were directly delivered to the tumors for each group. Mice were harvested on day 17 and photo of mouse was taken along with mouse tumor weight. Compared to control, SN12C xenograft mouse model showed 75% decrease in tumor weight in GRS and peptide injected group, respectively (Fig. 7A-C). Mouse injected with GRS or peptide showed no changes in mouse weight change suggesting lack of toxicity (Fig. 7D). For RENCA xenograft mouse model, GRS and peptide had no effect toward tumor growth (Fig. 8A-C) and had no toxicity (Fig. 8D).

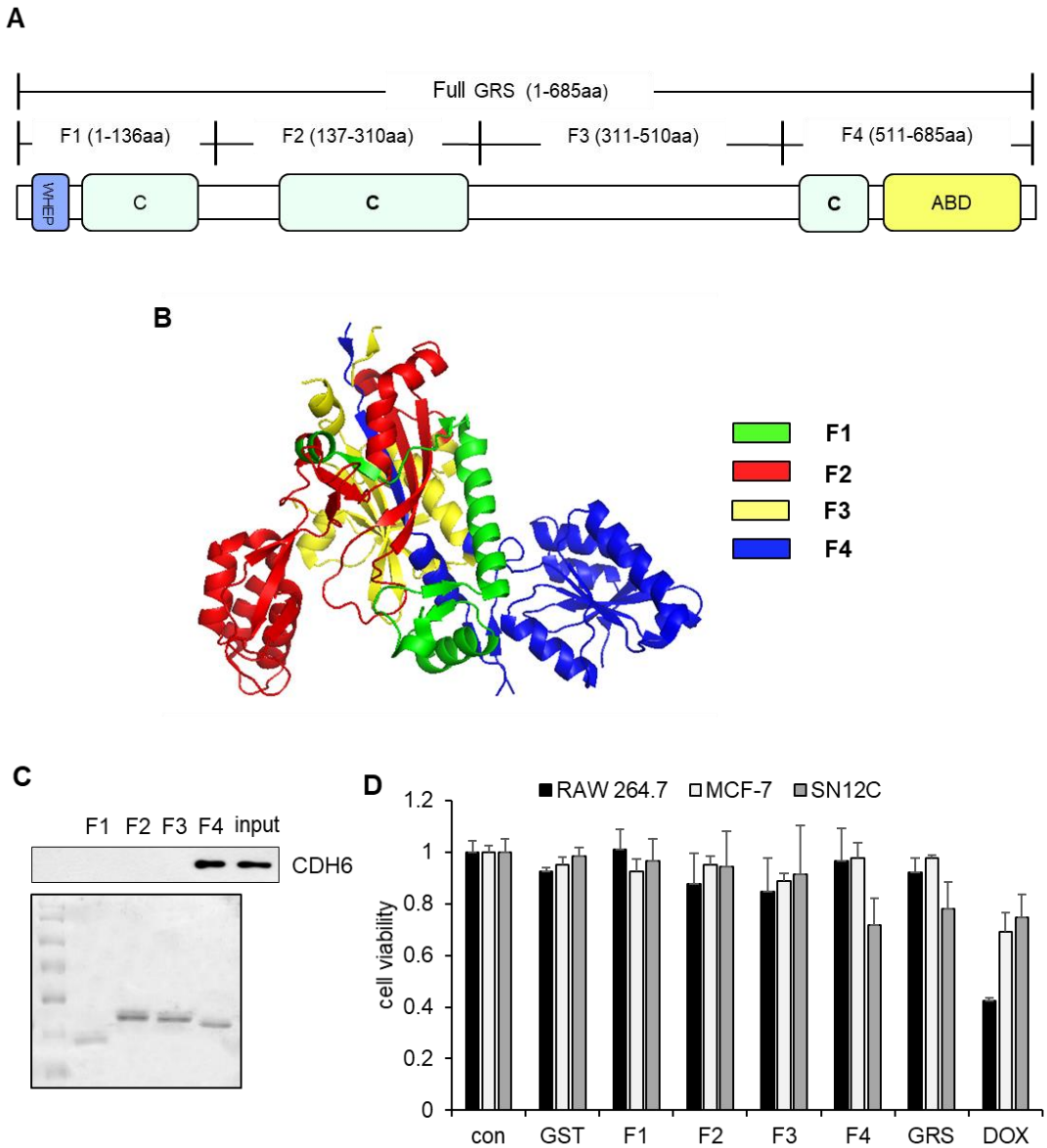


**Figure 1. GRS derived fragment 4(F4) induces tumor regression by binding to CDH6.** (A)Schematic representation for dividing full length GRS into four fragments sustaining WHEP, Catalytic, and Anti-codon Binding Domain**.** (B) Each GRS fragment was presented with different color in GRS full-length structure model. (C) GRS four fragments were purified along with GST-empty vector,

CDH6 binding to fragments was tested using pull-down assay and western blotted.

(D) Effect of GRS fragments on cell viability was tested using RAW264.7, MCF-7 and SN12C cell lines

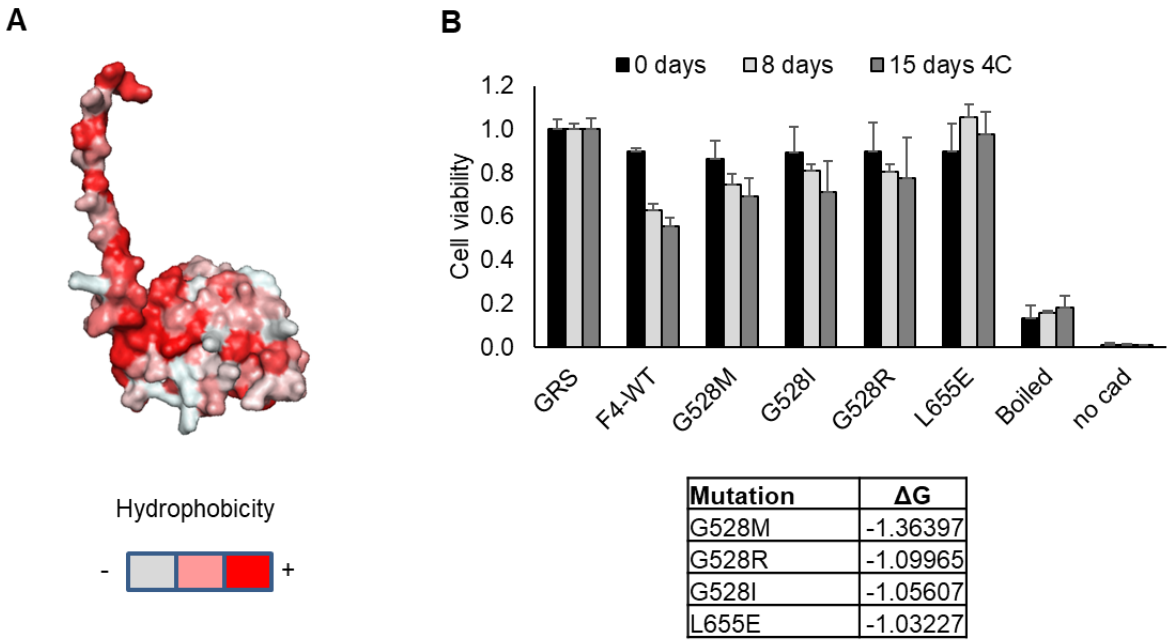


| Mutation | ΔG |
|---|---|
| G528M | -1.36397 |
| G528R | -1.09965 |
| G528I | -1.05607 |
| L655E | -1.03227 |

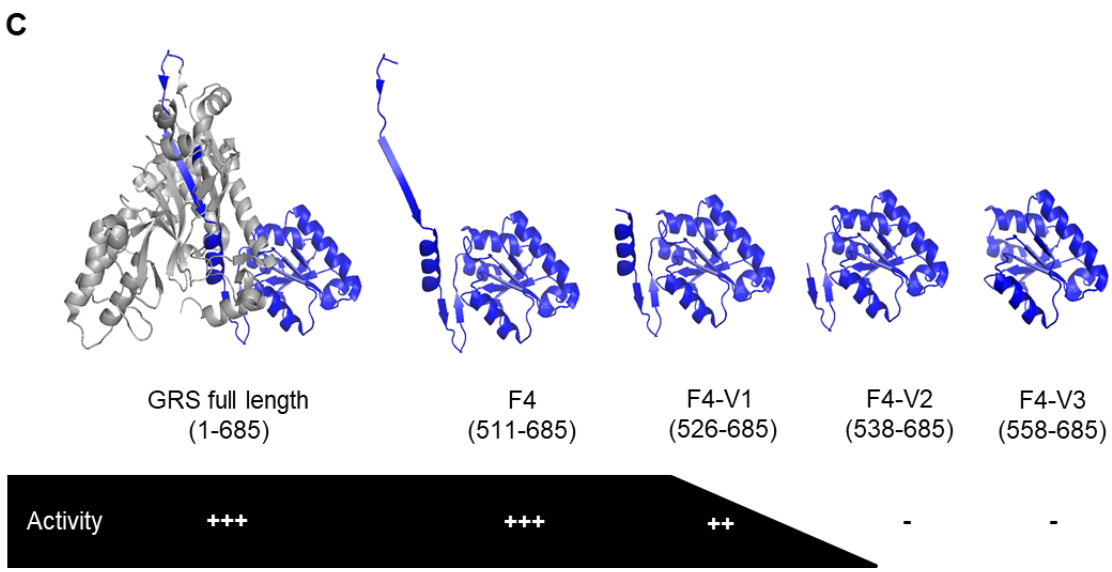

**Figure 2. Analysis of F4 fragments to improve efficancy** (A) Hydrophobicity model of F4 fragment (B) Point mutation based on delta G and binding was monitored at 0, 8, 15 days (C) Structure model of each N-terminal truncated of F4. Full length GRS, F4, F4-V1, F4-V2, and F4-V3 were designed and cell viability was tested to determine their efficacy. **Collaboration with Young Ho Jeon*.

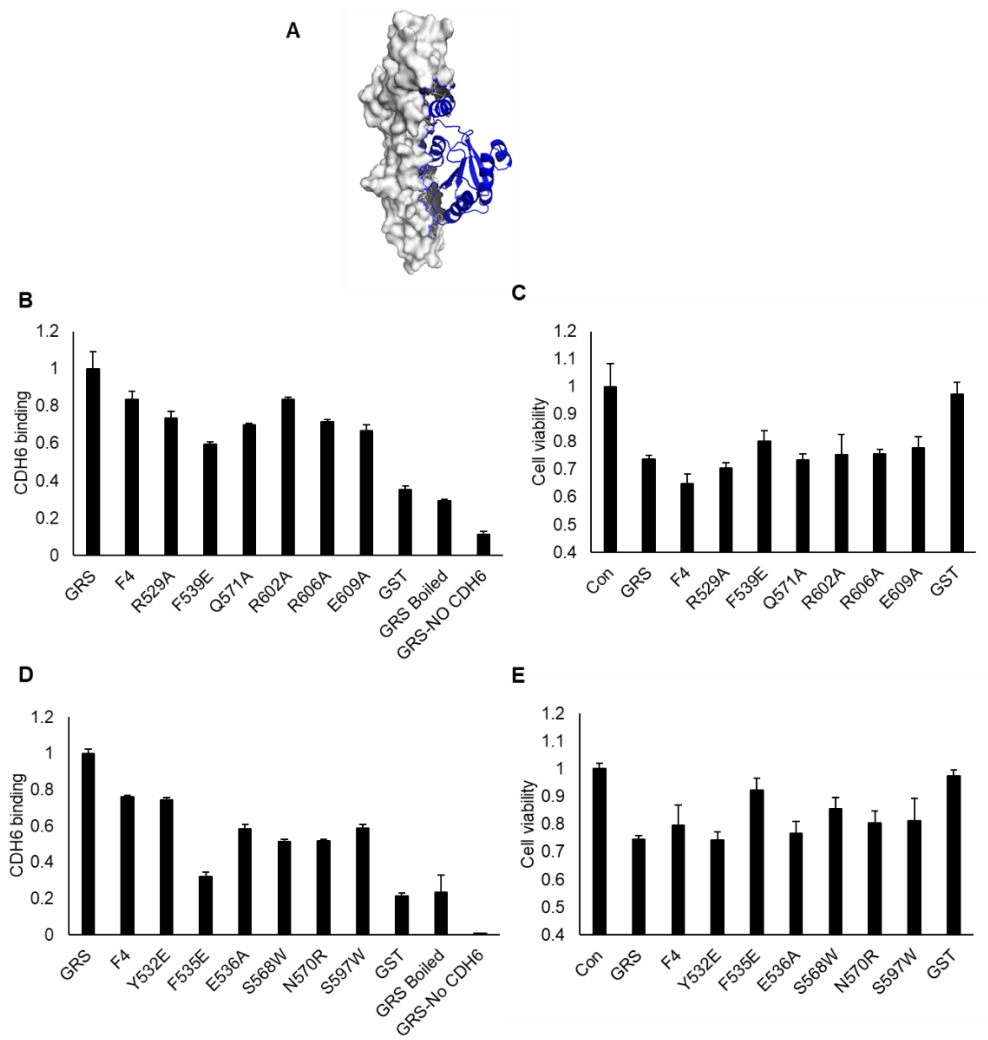


**Figure 3. Structure-based docking model predicts the binding site of F4 and CDH6 confirmed by *in-vitro* (A)** Crystal structure for CDH6 and GRS F4 were recovered from the protein data bank. Using HADDOCK 2.2, 12 poses of rigid

body docking were found, followed by semi-flexible docking with different side-chain rotamers. From 12 poses, Amber 14 was used to finalize docking model based on calculation of buried surface area that has short (10ns) molecular dynamics simulation. Based on docking model, predicted binding site were mutated for disrupt the binding interface. (B) Having GRS as positive control, F4 and F4 mutants were coated with 2 μg/ml and CDH6 (2 μg/ml) binding was tested using ELISA. (C) CDH6 expressing cell line, H460, was treated with 100 nM of F4 and F4 mutants for 24 h and the cell viability was measured by CCK8 assay. GRS 100 nM was used as positive control to induce cell death. (D) Peptide was coated with 2 μg/ml and checked CDH6 binding was tested using ELISA. GRS was used as a positive control. (E) CDH6 and pERK positive or negative cell lines were used to check cell viability using peptide 200 nM to see CDH6 dependency. Doxorubicin 100 nM was used as a positive control. * *Previously shown in Chanho Park's thesis* **Collaboration with Philip Kim*

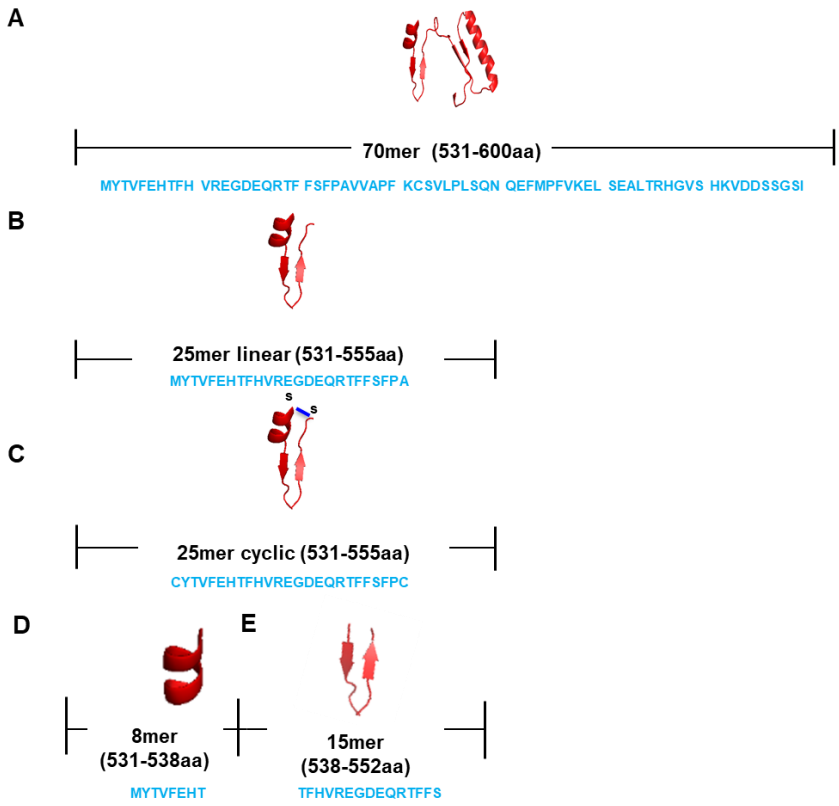


**Figure 4. Peptides were designed based on predicted active sites.** (A) 70mer (B) 25mer linear form without a linker. (C) 25 mer with added cysteine at the ends to form a cyclic peptide.(D) 8mer (E) 15mer

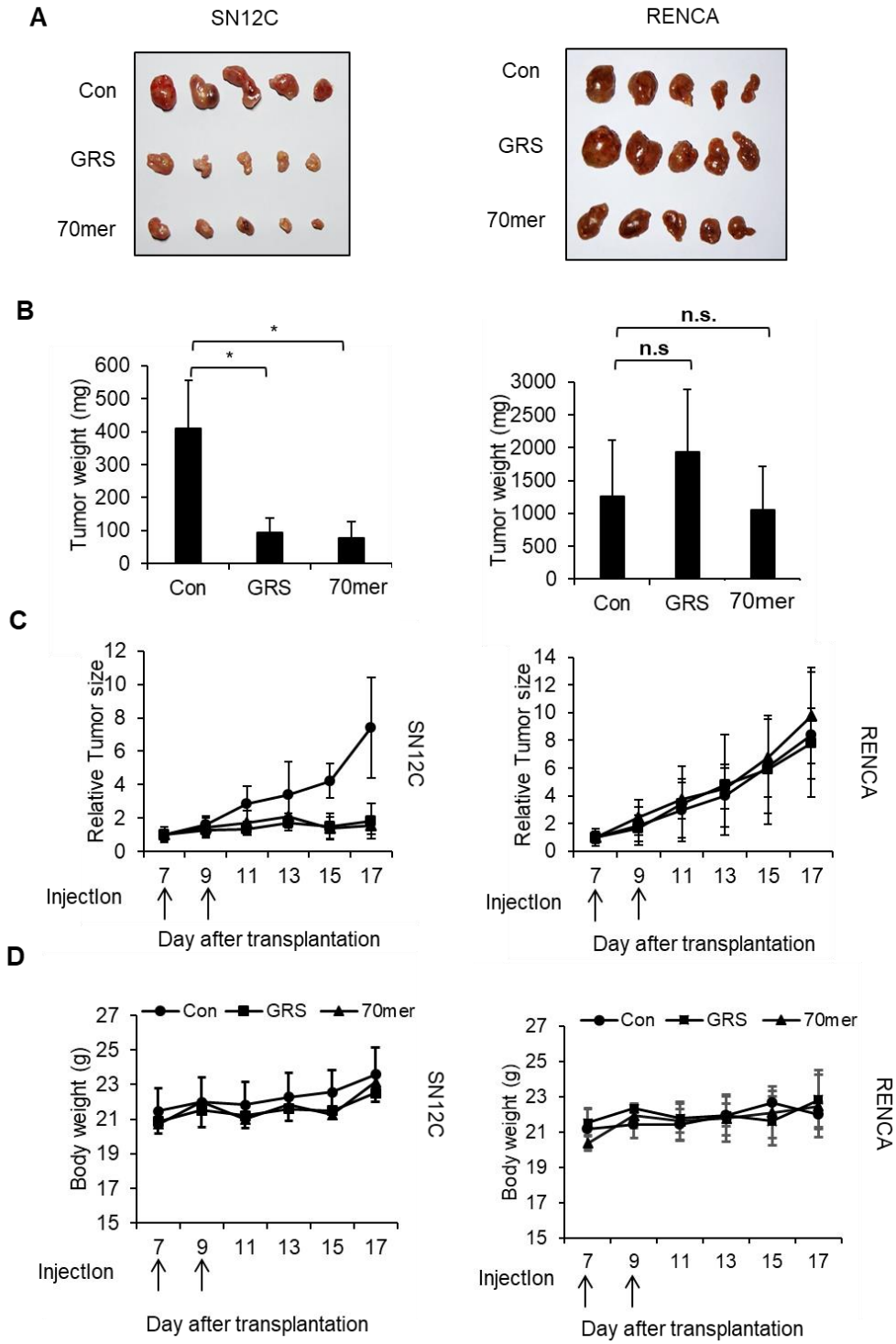
A
SN12C
RENCA
Con
GRS
70mer
B
Tumor weight (mg)
n.s.
n.s
C
Relative Tumor size
SN12C
RENCA
Injection
Day after transplantation
D
Body weight (g)
Con
GRS
70mer

**Figure 5. Peptide induces tumor regression in CDH6 positive cancer cells only** ***in vivo*** CDH6 positive cells, SN12C, were subcutaneously injected into the BALB/c nude mice and grown for 7 days until average tumor size reach 100 $mm^3$. PBS, GRS (20 μg) and Peptide (20 μg) were intra-tumor injected (*n*=5, animal/group) day 7 and 9. Tumor volume was calculated as the longest diameter x the shortest $diameter^2$ x 0.52. (A) Photographs of SN12C and RENCA xenograft tumors of PBS, GRS and peptide treated on day 7 and day 9 and monitored for 10 days. Tumor weight and size were measured on the last day. (B, C) The mouse weight was monitored and recorded every other day.

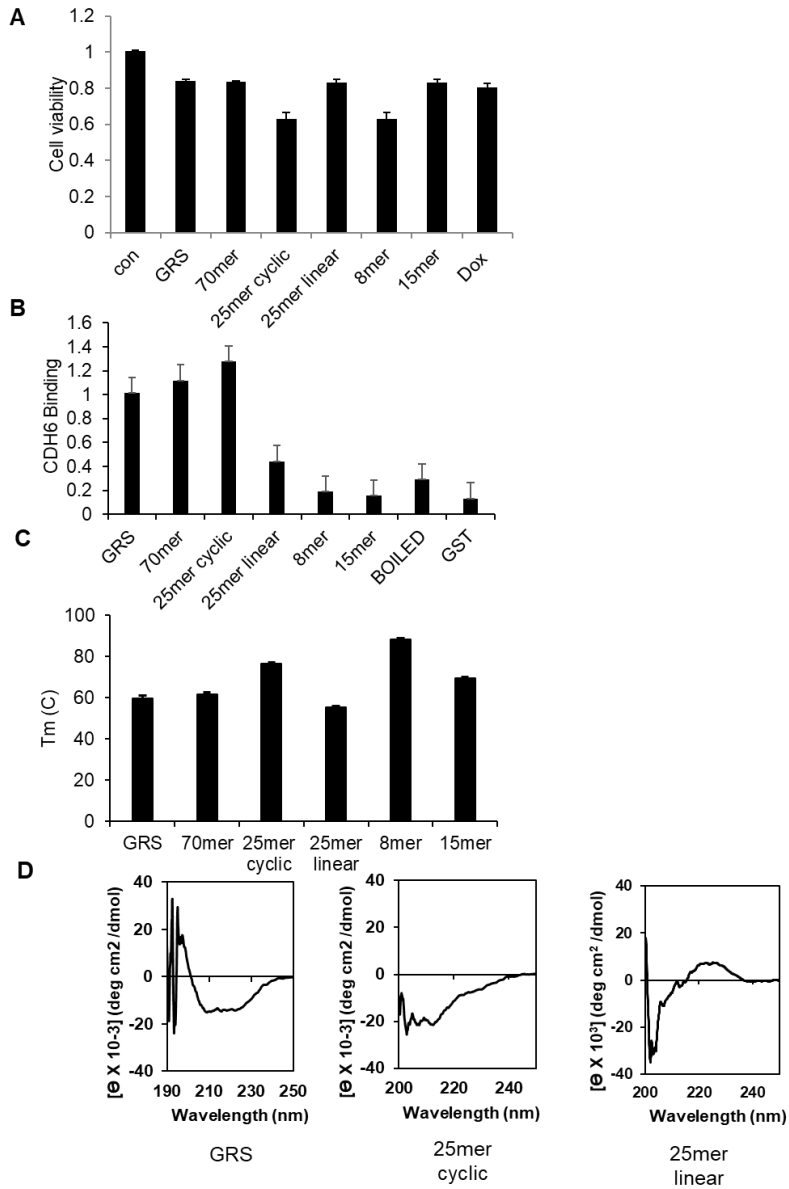


**Figure 6. *In-vitro* experiments testing the activity and stability of designed peptides.** (A)Peptide were treated H460 cells to monitor their effect on cell viability (B) ELISA plate was coated with peptides to analyze the binding effect to CDH6. (C) The peptides Tm was measured using thermal shift assay. (D) CD

spectrometery was peformed to show the 2D structure of the peptides

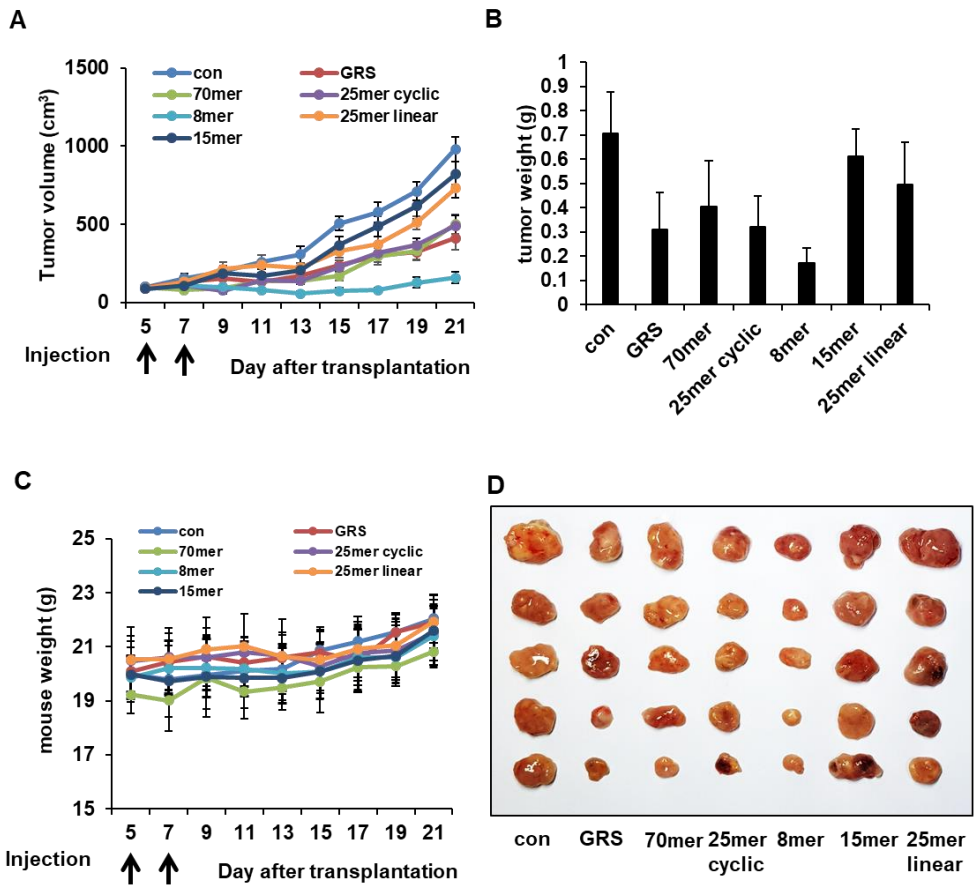


**Figure 7. GRS-derived small peptides induce tumor regression intra-tumor injection.** CDH6 positive cells, SN12C, were subcutaneously injected into the BALB/c nude mice and grown for 5 days until average tumor size reach 100 $mm^3$. PBS, GRS, 70mer, 25mer cyclic, 25mer linear and 8mer peptides (20 μg) were intra-tumor injected ($n$=5, animal/group) day 5 and 7. Tumor volume was calculated as the longest diameter x the shortest $diameter^2$ x 0.52. (A, B) Tumor weight and size were measured on the last day. (C) Mouse weight was monitored

during tumor growth (D) Photographs of SN12C xenograft tumors of PBS, GRS and peptides.

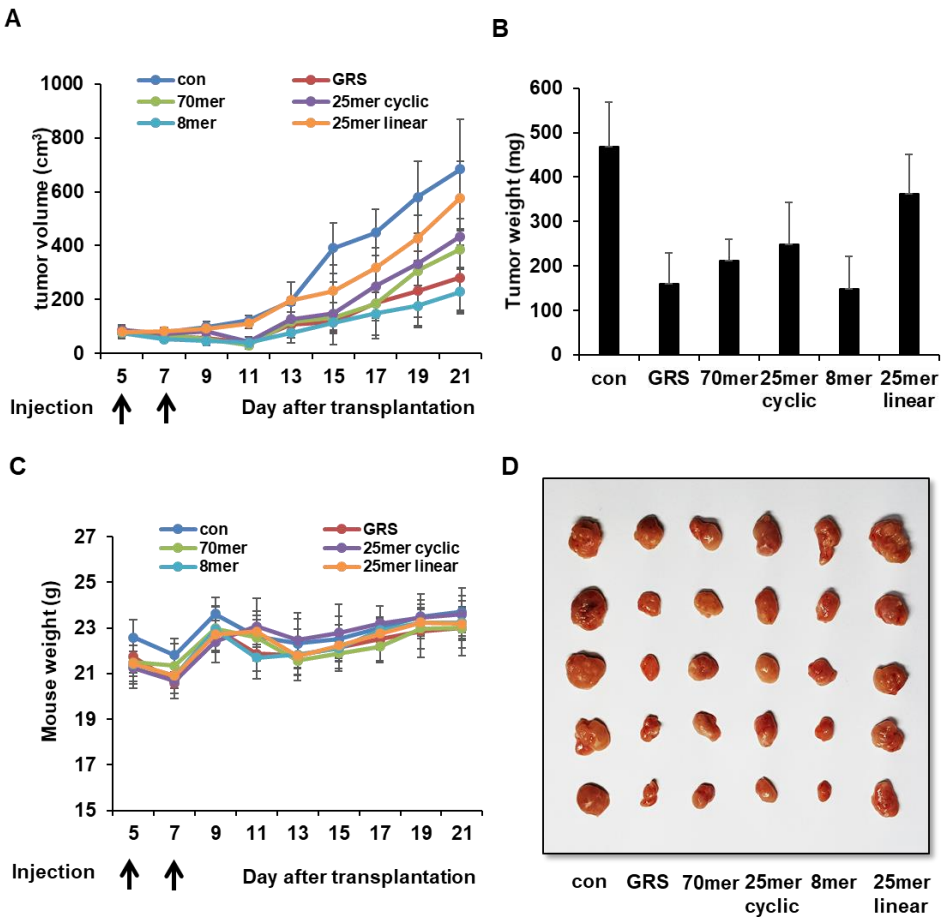


**Figure 8. GRS-derived small peptides induces tumor regression intra-venous injection.** CDH6 positive cells, SN12C, were subcutaneously injected into the BALB/c nude mice and grown for 5 days until average tumor size reach 100 $mm^3$. PBS, GRS, 70mer, 25mer cyclic, 25mer linear and 8mer peptides (20 μg) were intra-tumor injected ($n$=5, animal/group) day 5 and 7. Tumor volume was calculated as the longest diameter x the shortest $diameter^2$ x 0.52. (A, B) Tumor

weight and size were measured on the last day. (C) Mouse weight was monitored during tumor growth (D) Photographs of SN12C xenograft tumors of PBS, GRS and peptides

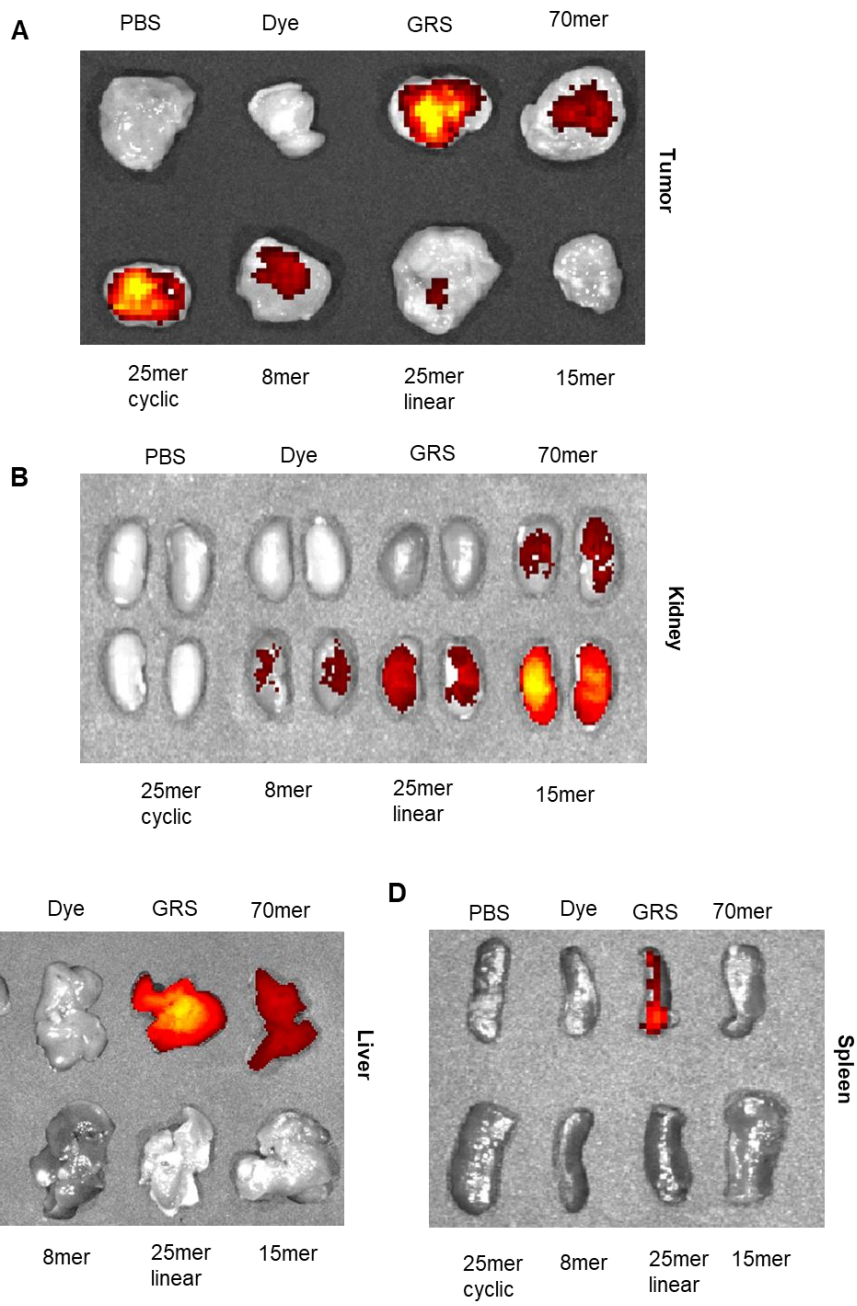

**Figure 9. Labeled GRS-derived small peptides target tumor cells.** GRS and GRS derived peptides were labeled with Alexa-fluor 590 were intravenously injected into balb/c nude mice. (A) Tumors were excised from mice and in vivo imaging system (IVIS) was used to monitor fluorescent activity. (B, C, D) The fluorescent was measured in the kidney, liver and spleen.

# DISCUSSION

Peptides are up-rising alternative targeting agents for human cancers (1). Peptide can resolve the problems that antibodies are facing, such as large size and nonspecific uptake by the reticuloendothelial system and liver (17). Antibodies are used for blocking the signal in cancer therapy, but peptides are used to activate signaling pathway through receptor binding. Development of peptides that activate the signal pathways by blocking tumor growth or inducing apoptosis can be a strategy used for cancer therapy (18). Peptide targeting cancer has been approved by Food and Drug administration (FDA) for past few years (2). Octreotide, a first approved peptide targeting somatostain receptor have been used for treating acromegaly and symptoms in cancer patient. Since then, more than 60 peptide drugs have been approved by FDA and more than 140 peptide drugs are in clinical trials (19). Therefore, targeting cancer using peptide can minimize side effects and can be beneficial for therapeutic drug development.

GRS has been shown to have an anti-tumor effect through CDH6 binding by dephosphorylation of ERK. Therefore, finding CDH6 binding domain of GRS is important for development of peptide drug targeting CDH6/PP2A/ERK axis for cancer therapy (7). GRS binding receptor Cadherin-6, type II classical cadherin family, have been found preferentially expressed in kidney. Kidney cancer

expresses higher level of CDH6 compare to normal (12, 20). Recently, antibody drug conjugate (ADC) targeting CDH6 for having high expression level in renal cancer are in clinical trial for targeting renal cancer drug (21). The drug development targeting renal cancer using CDH6 can be effective having high expression of CDH6 compare to normal.

For therapeutic peptide development, anti-tumor or pro-tumor protein has been developed into peptide. Peptide derived from EGFR, P53, Bcl-2 and CXC chemokine is being developed into anti-tumor peptide for cancer treatment (22, 23). P53-derived peptide has been developed in order to induce necrosis of cancer cell developing mdm-2 binding site inducing mdm-2 and P53 competition and CKC chemokine derived peptide blocks basic components of angiogenesis (24, 25). Therefore, developing GRS binding domain into peptide for inducing cancer cell apoptosis through CDH6 binding. GRS-derived peptide that has anti-tumor activity for the development of renal cancer therapeutic drug.

To determine CDH6 binding domain, GRS was divided into four fragments maintaining all existing domain and only fragment 4 (F4) showed CDH6 binding and anti-tumor activities *in vitro* and *in vivo*. Due to F4 poor stability, N-terminal of F4 inserted area of GRS and F4 fragment with different length of N-terminal truncated forms were designed in order to increase stability (26). As N-

terminal gets truncated, the activity of F4 decreased. These results gave an idea that the CDH6 binding domain may exist around N-terminal region of F4. To delineate the CDH6 binding domain, potential docking interface of CDH6/F4 complex were predicted using Haddock 2.2 (14). Predicted binding residues were mutated and F535, S568 and N570 residues showed loss of CDH6 binding and activity. For confirm binding domain, double point mutation was performed to increase disruption in CDH6 binding and F535 residue has been found to be critical for CDH6 binding.

Based on the docking model prediction, peptide was developed having alpha helix segment on both ends and beta-strand-loop-beta strand to maintain stability and conformation (27, 28). Peptide showed CDH6 binding and CDH6 dependent anti-tumor effects in dose dependent manner through dephosphorylation of ERK signal. Through mouse xenograft model, peptide showed tumor regression effect only toward CDH6 positive renal cancer cell. As a result, GRS-derived peptide showed binding toward CDH6 and anti-tumor effect toward renal cancer cell *in vitro* and *in vivo*.

GRS-derived peptide has high possibility for renal cancer therapeutic drug development. Current cancer treatments are chemotherapy and/or radiation therapy, but the side effects caused by immune response or non-specific treatments limit the

effectiveness of the cancer therapy (29, 30). Peptides have low toxicity and the ability to bind to different receptor for activating anti-tumor signaling are being magnified for the promising therapeutic drug (31). Renal cell cancer (RCC) is known for aggressive cancer that arises from the proximal renal tubular epithelium of the kidney and there are no specific RCC targeting drug (32). GRS-derived peptide can be used for the RCC specific targeting drug, having anti-tumor effect through binding to CDH6, which is highly expressed in renal cell cancer. Peptide can be used for the RCC therapeutic drug having CDH6 specificity and advantage of low toxicity of peptide. In this study, full length GRS was developed into 8 and 25 amino acids peptide sustaining anti-tumor effect by binding to CDH6 through dephosphorylation of ERK signaling. Also, it was shown the GRS peptide *in vivo* suppressed CDH6-positive tumor growth with low toxicity. This shows that GRS derived peptide is good drug candidate for cancers expressing CDH6.

Peptides are up-rising alternative targeting agents for human cancers (1). Peptide can resolve the problems that antibodies are facing, such as large size and nonspecific uptake by the reticuloendothelial system and liver (17). Antibodies are used for blocking the signal in cancer therapy, but peptides are used to activate signaling pathway through receptor binding. Development of peptides that activate the signal pathways by blocking tumor growth or inducing apoptosis can be a

strategy used for cancer therapy (18). Peptide targeting cancer has been approved by Food and Drug administration (FDA) for past few years (2). Octreotide, a first approved peptide targeting somatostain receptor have been used for treating acromegaly and symptoms in cancer patient. Since then, more than 60 peptide drugs have been approved by FDA and more than 140 peptide drugs are in clinical trials (19). Therefore, targeting cancer using peptide can minimize side effects and can be beneficial for therapeutic drug development.

GRS has been shown to have an anti-tumor effect through CDH6 binding by dephosphorylation of ERK. Therefore, finding CDH6 binding domain of GRS is important for development of peptide drug targeting CDH6/PP2A/ERK axis for cancer therapy (7). GRS binding receptor Cadherin-6, type II classical cadherin family, have been found preferentially expressed in kidney. Kidney cancer expresses higher level of CDH6 compare to normal (12, 20). Recently, antibody drug conjugate (ADC) targeting CDH6 for having high expression level in renal cancer are in clinical trial for targeting renal cancer drug (21). The drug development targeting renal cancer using CDH6 can be effective having high expression of CDH6 compare to normal.

For therapeutic peptide development, anti-tumor or pro-tumor protein has been developed into peptide. Peptide derived from EGFR, P53, Bcl-2 and CXC

chemokine is being developed into anti-tumor peptide for cancer treatment (22, 23). P53-derived peptide has been developed in order to induce necrosis of cancer cell developing mdm-2 binding site inducing mdm-2 and P53 competition and CKC chemokine derived peptide blocks basic components of angiogenesis (24, 25). Therefore, developing GRS binding domain into peptide for inducing cancer cell apoptosis through CDH6 binding. GRS-derived peptide that has anti-tumor activity for the development of renal cancer therapeutic drug.

To determine CDH6 binding domain, GRS was divided into four fragments maintaining all existing domain and only fragment 4 (F4) showed CDH6 binding and anti-tumor activities *in vitro* and *in vivo*. Due to F4 poor stability, N-terminal of F4 inserted area of GRS and F4 fragment with different length of N-terminal truncated forms were designed in order to increase stability (26). As N-terminal gets truncated, the activity of F4 decreased. These results gave an idea that the CDH6 binding domain may exist around N-terminal region of F4. To delineate the CDH6 binding domain, potential docking interface of CDH6/F4 complex were predicted using Haddock 2.2 (14). Predicted binding residues were mutated and F535, S568 and N570 residues showed loss of CDH6 binding and activity. For confirm binding domain, double point mutation was performed to increase

disruption in CDH6 binding and F535 residue has been found to be critical for CDH6 binding.

Based on the docking model prediction, peptide was developed having alpha helix segment on both ends and beta-strand-loop-beta strand to maintain stability and conformation (27, 28). Peptide showed CDH6 binding and CDH6 dependent anti-tumor effects in dose dependent manner through dephosphorylation of ERK signal. Through mouse xenograft model, peptide showed tumor regression effect only toward CDH6 positive renal cancer cell. As a result, GRS-derived peptide showed binding toward CDH6 and anti-tumor effect toward renal cancer cell *in vitro* and *in vivo*.

GRS-derived peptide has high possibility for renal cancer therapeutic drug development. Current cancer treatments are chemotherapy and/or radiation therapy, but the side effects caused by immune response or non-specific treatments limit the effectiveness of the cancer therapy (29, 30). Peptides have low toxicity and the ability to bind to different receptor for activating anti-tumor signaling are being magnified for the promising therapeutic drug (31). Renal cell cancer (RCC) is known for aggressive cancer that arises from the proximal renal tubular epithelium of the kidney and there are no specific RCC targeting drug (32). GRS-derived peptide can be used for the RCC specific targeting drug, having anti-tumor effect

through binding to CDH6, which is highly expressed in renal cell cancer. Peptide can be used for the RCC therapeutic drug having CDH6 specificity and advantage of low toxicity of peptide.

In this study, full length GRS was developed into 8 and 25 amino acids peptide sustaining anti-tumor effect by binding to CDH6 through dephosphorylation of ERK signaling. Also, it was shown the GRS peptide *in vivo* suppressed CDH6-positive tumor growth with low toxicity. This shows that GRS derived peptide is good drug candidate for cancers expressing CDH6

# MATERIALS AND METHODS

## Cell culture and materials

H460, HCT116, and RENCA cells were grown in RPMI1640 medium and SN12C, MCF7 and HeLa cells were grown in DMEM. Cells were grown with 10% fetal bovine serum with 1% antibiotics at 37°C in a 5% $CO_2$ incubator.

## Cell viability assay

H460, HCT116, MCF7, HeLa, SN12C or RENCA cell line were seeded into 96 well plate, 5000 cells/ml. Proteins were treated after 2 h with 100 µl serum free condition and incubated for 24 h. After 24 h, Cell Counting Kit-8 (CCK-8) assay (Dojindo Laboratories, Kumamoto, Japan) was performed. 10 µl of CCK8 solution was treated and after 1h O.D values was measured using microplate-reader (TECAN, Mannedorf, Swiss) at 450 nm.

## Mutagenesis

Followed site-directed mutagenesis kit instructions (Agilent, Santa Clara, CA, USA). Primers were designed accordingly 37 mer with Tm greater than 78°C. For each mutant, 30 ng of F4 mutant DNA, 125 ng of primers, 2.25 mM of dNTP, 10x reaction buffer and 2.5 U/µl Pfu were mixed. Mixing and spinning down, PCR for 95°C for 30 s, then 95°C for 30 s, 55°C for 1 min and 11 min 68°C for 18 cycles were performed. The reaction was then digested with 10U Dpn I for 37°C for 1 hour.

**F4 Protein purification (Batch)**

Transformation was performed into BL21 competent cell. After spreading into ampicillin plus agar plate, plate was incubated at 37°C overnight. Colony was picked into 3 ml of LB plus ampicillin and up-scaled into 1 L at 37°C. When O.D value reached 0.6, 1 mM of IPTG (Sigma, St. Louis, MO) was added and incubated overnight at 18°C. At 3500 rpm centrifugation for 30 min and pellet was collected using 7.8 pH buffer. 9 times of sonification were performed and centrifuged for 30 min at 13000 rpm. Supernatant were collected and it was bound to 300 µl of glutathione agarose beads (Thermo, Waltham, MA) for 4 h or overnight. The beads were washed 3 times with 8 ml of PBS and eluted with 500 µl of 40 mM pH 8.0 L-Glutathione reduced (Sigma) for 2 to 4 hr. The protein was dialyzed in PBS-15% glycerol two times, 2 and 6 h or overnight respectively, and harvested. The protein concentrations were measured using protein dye reagent (BioRad, Hercules, CA) at 595 nm spectrometer (Eppendorf, Hamburg, German) and purity was checked by Coomassi staining.

**CDH6 Protein purification (column)**

Pkk-CDH6-Fc vector (250 µg/100 ml) was transfected into HEK293F cells (2 x $10^6$ cells/ml) using Linear PEI (Polysciences, Warrington, PA). Cell was cultured at GIBCO Freestyle™ 293 (TECAN, Mannedorf, Swiss) media for 6 days in 8% $CO_2$, 37°C. After 6 days of culture, supernatant was collected and centrifuged 2400 rpm

for 15 min. Using bottle-top filter (Corning, Kennebunk, ME), supernatant was filter. Using CDH6 (100 ml) supernatant was bound to prewashed 250 µl Protein G agarose beads (Invitrogen, Carlsbad, CA) with 5 ml PBS for three times. The flow through was collected and reloaded to ensure proper binding of CDH6 to beads. The beads were then washed with 5 ml of PBS for a total of three washings. CDH6 was then eluted with 200 µl of 100 nM Glycine pH 2.5 (Affymetrix, Santa Clara, CA) into 20 µl 1M Tris pH 8.8 (Duchefa Biochemie, Haarlem, Netherlands) for neutralization and this step was repeated four times for a total of six elutions. The protein concentrations were measured using protein dye reagent (BioRad, Hercules, CA) at 595 nm spectrometer (Eppendorf, Hamburg, German) and higher concentrations were pooled. The protein was dialyzed in PBS-15% glycerol two times, 2 and 6 h or overnight respectively, and harvested.

**Haddock 2.2 docking program**

Crystal structures for CDH6 (pdb id: 3lnd, chain A) and GRS F4 (pdb id: 2pme, residues 256-674) were recovered from the protein data bank. Missing residues were modeled in to both structures using Modeler (15). Energy minimization was carried via the steepest descent and conjugate gradient methods using the Amber 14 molecular modeling package (16). Potential CDH6/F4 complexes were predicted using the protein–protein docking software HADDOCK2.2 (High

Ambiguity Driven protein-protein DOCKing) (14). HADDOCK was used to generate 12 poses using rigid body docking, followed by semi-flexible docking with different side-chain rotamers. Each of the 12 poses was evaluated by visual inspection together with buried surface area calculations before and after a short (10 ns) MD simulation using Amber 14. The most stable and biologically realistic complex was thereby selected and used to predict interface mutations that may adversely affect binding.

**Pulldown assay**

Purified protein 4 μg and 30 μl of glutathione agarose beads (Thermo, Waltham, MA) were incubated for 2 h at 4°C. After three times of PBS washing, CDH6 2 μg was added and incubated for 4 h at 4°C. After the incubation samples were washed with PBS five times and boiled for 15 min. Sample was analyzed with 10% SDS-PAGE and gel stained with Coomassie, followed by immunoblot analysis using anti-human antibody, 1:10000 (Thermo, Waltham, MA).

**Protein stability test**

Followed Proteostat Thermal shift stability assay kit instruction (Enzo Life Sience, Farmingdale, NY) 2 μg of protein was added with 2 μl of dye and 10x reaction buffer total volume of 20 μl. Each tube was mixed using pipet and transferred into qRT-PCR plate. Samples were analyzed by Texas Red dye increasing the

temperature from 25 to 99°C with 0.3% degree difference in minutes. Experiment was performed using Thermal cycler dice™ Real Time system (Takara, Shiga, Japan) to find melting temperature for each protein and peptide.

**Xenograft Mice model**

Animal experiments were performed using the University Animal care and committee guidelines at Seoul Nation University. The tumorigenicity of HCT116, SN12C, and RENCA were tested using BALB/c nude female mice. $3 \times 10^7$ cells were injected to each mouse using a 20-gauge needle and allowed to grow up to 100 $mm^3$. Tumor growth was checked every 2 days, and when the tumor formation was observed using a caliper to measure tumor size. (Tumor volume was calculated as length x $width^2$ x 0.52). When tumor size reached 100 $mm^2$, proteins were injected in first day. Tumor weight and size were monitored every 2 days up to 12 days after injection of proteins. After sacrifices, tumor weights were measured.

# REFERENCES


1. Craik DJ, Fairlie DP, Liras S, & Price D (2013) The future of peptide-based drugs. *Chem Biol Drug Des* 81(1):136-147.

2. Adare A*, et al.* (2011) Measurements of higher order flow harmonics in Au+Au collisions at radicals(NN)=200 GeV. *Phys Rev Lett* 107(25):252301.

3. Kaspar AA & Reichert JM (2013) Future directions for peptide therapeutics development. *Drug Discov Today* 18(17-18):807-817.

4. Guo M, Yang XL, & Schimmel P (2010) New functions of aminoacyl-tRNA synthetases beyond translation. *Nat Rev Mol Cell Biol* 11(9):668-674.

5. Kim S, You S, & Hwang D (2011) Aminoacyl-tRNA synthetases and tumorigenesis: more than housekeeping. *Nat Rev Cancer* 11(10):708-718.

6. Wakasugi K & Schimmel P (1999) Two distinct cytokines released from a human aminoacyl-tRNA synthetase. *Science* 284(5411):147-151.

7. Park MC*, et al.* (2012) Secreted human glycyl-tRNA synthetase implicated in defense against ERK-activated tumorigenesis. *Proc Natl Acad Sci U S A* 109(11):E640-647.

8. Chitaev NA & Troyanovsky SM (1997) Direct Ca2+-dependent heterophilic interaction between desmosomal cadherins, desmoglein and

desmocollin, contributes to cell-cell adhesion. *J Cell Biol* 138(1):193-201.

9. Wheelock MJ & Johnson KR (2003) Cadherin-mediated cellular signaling. *Curr Opin Cell Biol* 15(5):509-514.

10. Nollet F, Kools P, & van Roy F (2000) Phylogenetic analysis of the cadherin superfamily allows identification of six major subfamilies besides several solitary members. *J Mol Biol* 299(3):551-572.

11. Angst BD, Marcozzi C, & Magee AI (2001) The cadherin superfamily: diversity in form and function. *J Cell Sci* 114(Pt 4):629-641.

12. Patel SD, Chen CP, Bahna F, Honig B, & Shapiro L (2003) Cadherin-mediated cell-cell adhesion: sticking together as a family. *Curr Opin Struct Biol* 13(6):690-698.

13. Zuiderweg ER (2002) Mapping protein-protein interactions in solution by NMR spectroscopy. *Biochemistry* 41(1):1-7.

14. Dominguez C, Boelens R, & Bonvin AM (2003) HADDOCK: a protein-protein docking approach based on biochemical or biophysical information. *J Am Chem Soc* 125(7):1731-1737.

15. Fiser A, Do RK, & Sali A (2000) Modeling of loops in protein structures. *Protein Sci* 9(9):1753-1773.

16. D. A. Case VB, J. T. Berryman, et al. (2014) *Amber 14*.

17. Chames P, Van Regenmortel M, Weiss E, & Baty D (2009) Therapeutic

antibodies: successes, limitations and hopes for the future. *Br J Pharmacol* 157(2):220-233.

18. Boohaker RJ, Lee MW, Vishnubhotla P, Perez JM, & Khaled AR (2012) The use of therapeutic peptides to target and to kill cancer cells. *Curr Med Chem* 19(22):3794-3804.

19. Fosgerau K & Hoffmann T (2015) Peptide therapeutics: current status and future directions. *Drug Discov Today* 20(1):122-128.

20. Paul R*, et al.* (1997) Cadherin-6, a cell adhesion molecule specifically expressed in the proximal renal tubule and renal cell carcinoma. *Cancer Res* 57(13):2741-2748.

21. Bialucha CU*, et al.* (2017) Discovery and Optimization of HKT288, a Cadherin-6 Targeting ADC for the Treatment of Ovarian and Renal Cancer. *Cancer Discov*.

22. Kolluri SK*, et al.* (2008) A short Nur77-derived peptide converts Bcl-2 from a protector to a killer. *Cancer Cell* 14(4):285-298.

23. Ofuji K*, et al.* (2015) A peptide antigen derived from EGFR T790M is immunogenic in non-small cell lung cancer. *International Journal of Oncology* 46(2):497-504.

24. Michl J*, et al.* (2006) PNC-28, a p53-derived peptide that is cytotoxic to cancer cells, blocks pancreatic cancer cell growth in vivo. *Int J Cancer*

119(7):1577-1585.

25. Karagiannis ED & Popel AS (2008) Novel anti-angiogenic peptides derived from ELR-containing CXC chemokines. *J Cell Biochem* 104(4):1356-1363.

26. Lu Z, Wang Q, Jiang S, Zhang G, & Ma Y (2016) Truncation of the unique N-terminal domain improved the thermos-stability and specific activity of alkaline alpha-amylase Amy703. *Sci Rep* 6:22465.

27. Errington N, Iqbalsyah T, & Doig AJ (2006) Structure and stability of the alpha-helix: lessons for design. *Methods Mol Biol* 340:3-26.

28. Doig AJ & Baldwin RL (1995) N- and C-capping preferences for all 20 amino acids in alpha-helical peptides. *Protein Sci* 4(7):1325-1336.

29. Luo Y & Prestwich GD (2002) Cancer-targeted polymeric drugs. *Curr Cancer Drug Targets* 2(3):209-226.

30. Li C (2002) Poly(L-glutamic acid)--anticancer drug conjugates. *Adv Drug Deliv Rev* 54(5):695-713.

31. Xiao YF*, et al.* (2015) Peptide-Based Treatment: A Promising Cancer Therapy. *J Immunol Res* 2015:761820.

32. Gupta K, Miller JD, Li JZ, Russell MW, & Charbonneau C (2008) Epidemiologic and socioeconomic burden of metastatic renal cell carcinoma (mRCC): a literature review. *Cancer Treat Rev* 34(3):193-205.

33. Zhang Q, Zeng SX, & Lu H (2015) Determination of Maximum Tolerated Dose and Toxicity of Inauhzin in Mice. *Toxicol Rep* 2:546-554.

# 요약 (국문초록)

# Glycyl-tRNA Synthetase 펩타이드의 항암효과에 관한 연구

서울대학교

융합과학기술대학원

분자의학 및 바이오제약학과 의약생명과학전공

Peter Goughnour

우리는 대식세포에서 나온 GRS단백질이 종양형성에서 중요한 면역감시기능에서 역할이 있다는 점을 보여주었다. GRS는 선천면역과 종양세포 사멸에 관여하는 것을 확인 하였다. 또한 GRS 유래 펩타이드를 통해 종양치료에 쓰일수 있는 신약개발 후보군을 개발하였다.

ARSs 단백질은 세포 내에서 tRNA에 상보적인 아미노산을 붙여주는 역할을 하며 단백질 합성에 중요한 효소로 알려져 있다. 근래에 들어 ARSs 들은 기존에 알려진 역할 이외에도 전사과정, 세포증식, 면역염증, 혈관 형성, 그

리고 세포사멸 등 여러 가지 기능을 하는 것으로 연구되고 있다. 이번 연구는 GRS와 GRS유래 펩타이드가 종양형성에서 미치는 영향에 대해 집중하여 진행을 하였다.

첫 번째 파트에선, GRS가 스트레스 상황이 왔을 때 대식세포로부터 분비되는 것을 확인 하였고 자가 분비 역할로써 CELSR2에 붙는 결과를 확인하였다. GRS가 CELSR2를 통하여 대식세포에 붙음으로써 MEK 신호전달 경로를 활성화 시켰으며 관련된 사이토카인의 종류인 TNF-α, IL-6, 그리고 CXCL10들이 증가함을 확인하였다. 결과적으로 대식세포는 M0에서 항암작용을 나타내는 M1으로 바뀌었으며 그와 관련된 식 세포 활동을 확인하였다. 종양이 개시되는 쥐 모델에서 GRS가 종양의 성장을 억제시켰으며 이 결과는 GRS가 면역감시 역할에서 필요한 사이토카인으로써의 기능을 보여주었다.

두번째 파트에선 GRS의 활성 도메인을 이용하여 펩타이드 약물을 개발하였다. GRS는 알려져 있기로 CDH6를 발현하는 종양세포에 부착된 후 ERK 신호전달 경로를 억제하여 세포사멸을 유도하는 것으로 연구되었다. 돌연변이 생성작업을 통해 CDH6 에 결합하는 활성 도메인을 찾았으며 결과를 토대로 합성 펩타이드를 *in vitro*와 *in vivo*에서 시험해 보았다. 펩타이드는 아미노산 25개까지 줄였으며 in vivo에서 종양성장이 줄어드는 것을 정맥주사

방법을 통해 확인하였다. 이 결과를 토대로 펩타이드가 종양치료의 약물후보로 쓰일 수 있다는 가능성을 제시하였다.

주요어: Glycyl-tRNA synthetase, Macrophage, Cancer, Peptide, Therapeutic drug, Cadherin-6, CELSR2,

학번: 2010-31389